B
REVISED PROBABILISTIC ANALYSES FOR REACTOR PRESSURE VESSEL HEAD PENETRATION NOZZLES (RPVHPNS)

B.1 Introduction

This document includes revised input listings and results for the probabilistic RPVHPN assessment presented in Appendix B of MRP-335 Rev. 1 [1]. These results are provided in response to the second request for additional information (RAI) for MRP-335 Rev. 1 [2]. The updated inputs and results provided in this attachment will be incorporated in Appendix B of MRP-335 Rev. 2.

Detailed discussion of the probabilistic modeling methodology, incorporated models, and uncertainty propagation is provided in MRP-335 Rev. 1 [1] and will be included in the planned revision, MRP-335 Rev. 2. Parameter distributions, descriptions, and sources for all inputs used in the probabilistic assessment for RPVHPNs are provided in Section B.2, with base case inputs listed in Section B.2.1. Sensitivity studies are performed with respect to various model parameters to characterize the impact of modeling assumptions and input uncertainty on nozzle leakage and ejection risk predictions. The parameters varied by each of these cases are documented in Section B.2.2. Results for base cases and sensitivity cases are presented in Section B.3.

B.2 Probabilistic Model Inputs

B.2.1 Base Case Inputs

The probabilistic inputs and results presented in this attachment are designed to bound the conditions for all Alloy 600 reactor vessel top heads penetration nozzles in the U.S. that are being considered for peening mitigation. The inputs presented in this section correspond to the non-cold head (i.e., hot head) and cold head base cases.

These inputs typically represent best-estimate values, with input distributions applied to handle uncertainties. However, there are several factors that tend to make the analysis results and conclusions conservative:

- No credit is given to peening for slowing the growth of through-wall circumferential cracks along the weld contour of RPVHPNs.
- A through-wall 30° circumferential flaw located at the top of the weld is assumed to be produced immediately upon nozzle leakage (i.e., through-wall cracking to the nozzle annulus).

- No credit is given to peening for slowing the growth of axial through-wall cracks growing toward the nozzle OD annulus from the below the J-groove weld on RPVHPNs.
- Growth under the peening layer, which may manifest as balloon crack growth, is given full credit by neglecting peening stresses for the calculation of surface growth of cracks.
- No credit is taken for ET inspections.
- A UT POD of zero is assumed for flaws with depth less than 10% through-wall. Furthermore, the mean UT POD curve is assumed to have a flaw detection rate below that of the worst-case qualified UT detection instrument and inspector.
- No credit is taken for volumetric or surface leak path examinations.

Input values in Table B-1 through Table B-8 that are highlighted orange have different values for the hot head and cold head base cases.

B.2.1.1 Peening Residual Stress Effect

To accommodate the range of peening processes that may be applied, the inputs to the probabilistic assessment are the bounding values specified in the performance criteria listed in Attachment 2. Specifically, post-peening stress profiles (including peening stress on the surface with and without operating stresses), the depth of the compressive residual stress field, and the modeled inspection requirements are defined in Attachment 2. If a peening mitigation process meets these performance criteria, the results of this probabilistic assessment are applicable.

B.2.1.2 Crack Initiation Model

Another significant update to the model inputs is the use of the PWSCC initiation Weibull model presented in Appendix A of MRP-395 [3]. This is the latest available Weibull model for PWSCC initiation in CRDMs and reflects U.S. PWR operating experience through July 2014. Additional PWSCC indications in RPVHPNs that have been detected since July 2014 are consistent with this initiation model. Additionally, uncertainty in the updated Weibull model is captured in the Weibull characteristic time, rather than distributing uncertainty between the Weibull slope and characteristic time. Detailed discussion of the updated model and operating experience will be provided in MRP-335 Rev. 2.

B.2.1.3 UT Probability of Detection

Similar to past studies of PWSCC, crack inspection is modeled with POD curves that are functions of crack geometry (e.g., deeper cracks lead to a higher likelihood of detection).

The median UT inspection POD curve used for cracking on ID and OD locations of the RPVHPN tube is shown in Figure B-1. This curve was set based on the minimum qualification criteria specified in 10 CFR 50.55a as detailed in MRP-335 Rev. 1 appendix Section B.8.4.2. As with DM welds, the performance demonstration requirements for UT inspections of RPVHPNs do not include flaws shallower than 10% the wall thickness, so flaws with a depth up to 10% of the wall thickness are conservatively modeled to be undetectable (POD of 0). The probabilistic model does not include UT inspection for detection of cracking in RPVHPN J-groove welds.

B.2.1.4 Updates to Modeling Framework

The RPVHPN modeling framework used in generating the results in this attachment is identical to that used in MRP-335 Rev. 1 [1] except for the following changes:

- Includes ability to change BMV inspection interval after peening
- Includes ability to schedule multiple follow-up UT examinations subsequent to peening
- Includes ability to set the peening surface stress by deterministically specifying the sum of the post-peening residual stress and normal operating stress at the peened surface
- Includes modified POD curve capable of using a POD of zero for flaws depths below a given through-wall fraction

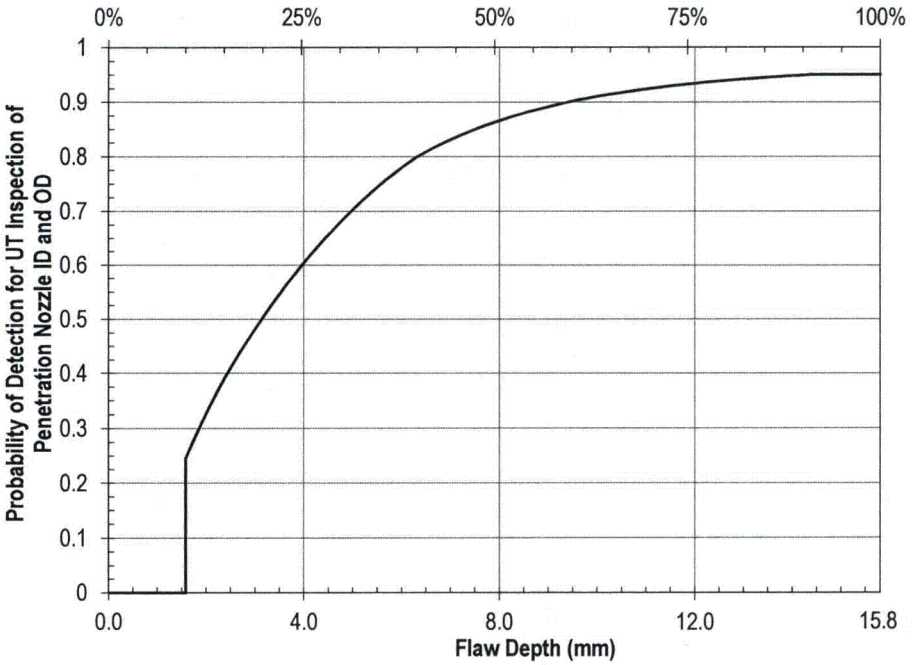

Figure B-1
Median Assumed UT Inspection POD Curve for Axial Cracking Initiating at the RPVHPN ID and OD

Table B-1
Summary of General Inputs

Symbol	Description	Source	Units	Parameter Type	Hot Head Base Case	Cold Head Base Case
	Total number of trials	Convergence Study	# trials		1.00E+06	1.00E+06
	Number of operating cycles	Selected to yield desired cumulative operating time	# cycles		30	30
	Nominal cycle length	Upper end of cycle length of U.S. PWRs	years		2	2
CF	Operating capacity factor	Representative capacity factor for U.S. PWR	-		0.97	0.97
	Cycle of first UT inspection	Based on typical operating reactor service histories	Cycle number		10	10
	Pre-peening UT inspection interval	ASME Code Case N-729-1	# cycles		1	3
	Pre-peening BMV inspection interval	ASME Code Case N-729-1	# cycles		1	2
T	Operating temperature	Selected based on properties of units serving as characteristic hot/cold head	°F	type	Normal	Normal
				mean	605	561
				stdev	5	5
				min	575	520
				max	635	600
N_{pen}	Number of modeled penetrations	Selected based on properties of units serving as characteristic hot/cold head	-		78	78
N_{flaw}	Maximum number of part-depth flaws modeled per penetration	Selected to capture PWSCC locations and mechanisms observed in industry RPVHPNs	-		6	6
t	Nozzle thickness	Representative of CRDM nozzle thickness of units serving as characteristic hot/cold head	in.		0.62	0.62
D_o	Nozzle outer diameter	Representative of CRDM nozzle OD of units serving as characteristic hot/cold head	in.		4.00	4.00
t_{head}	Reactor head thickness	Representative of industry PWRs	in.		5.98	5.98

Table B-2
Summary of Weld Geometry Inputs

Symbol	Description	Source	Units	Parameter Type	Hot Head Base Case	Cold Head Base Case
	Representative length from weld surface to weld root, uphill	Inputs to finite element analyses of J-groove weld residual stresses; distribution considers various penetration geometries	in.	type	Normal	Normal
				mean	1.05	1.05
				stdev	0.18	0.18
				min	0.50	0.50
				max	1.70	1.70
	Representative length from weld surface to weld root, downhill	Inputs to finite element analyses of J-groove weld residual stresses; distribution considers various penetration geometries	in.	type	Normal	Normal
				mean	0.97	0.97
				stdev	0.23	0.23
				min	0.50	0.50
				max	1.70	1.70
	Representative length from weld toe to weld root, uphill	Inputs to finite element analyses of J-groove weld residual stresses; distribution considers various penetration geometries	in.	type	Normal	Normal
				mean	1.38	1.38
				stdev	0.30	0.30
				min	0.80	0.80
				max	2.90	2.90
	Representative length from weld toe to weld root, downhill	Inputs to finite element analyses of J-groove weld residual stresses; distribution considers various penetration geometries	in.	type	Normal	Normal
				mean	1.36	1.36
				stdev	0.37	0.37
				min	0.80	0.80
				max	2.90	2.90
	Ratio of weld path length to weld half-width, uphill	Inputs to finite element analyses of J-groove weld residual stresses; distribution considers various penetration geometries	-		1.62	1.62
	Ratio of weld path length to weld half-width, downhill	Inputs to finite element analyses of J-groove weld residual stresses; distribution considers various penetration geometries	-		1.24	1.24
	Incidence angles for penetrations	Selected based on properties of units serving as characteristic hot/cold head	degrees		Discrete List	Discrete List

Table B-3
Summary of Loading Inputs for RPVHPN Model

Symbol	Description	Source	Units	Parameter Type	Hot Head Base Case	Cold Head Base Case
P_{op}	Normal operating pressure	Representative of industry PWRs	ksi		2.248	2.248
$f_{oper,ID}$	Nozzle ID operating hoop stress concentration factor	Finite element analyses of operational stresses on CRDM nozzle; across various penetration angles	-	type	Normal	Normal
				mean	3.480	3.480
				stdev	0.729	0.729
				min	0.000	0.000
				max	7.850	7.850

Table B-3
Summary of Loading Inputs for RPVHPN Model (Continued)

Symbol	Description	Source	Units	Parameter Type	Hot Head Base Case	Cold Head Base Case
$\sigma_{0,tot,1}$	Total hoop stress at penetration ID above weld	Finite element analyses of operational stresses on CRDM nozzle; across various penetration angles	ksi	type	Normal	Normal
				mean	40.99	40.99
				stdev	7.34	7.34
				min	0.00	0.00
				max	85.02	85.02
$\sigma_{0,tot,2}$	Total hoop stress at penetration OD below weld, uphill	Finite element analyses of operational stresses on CRDM nozzle; across various penetration angles	ksi	type	Normal	Normal
				mean	53.78	53.78
				stdev	9.92	9.92
				min	0.00	0.00
				max	113.30	113.30
$\sigma_{0,tot,3}$	Total hoop stress at weld surface center, uphill	Finite element analyses of operational stresses on CRDM nozzle; across various penetration angles	ksi	type	Normal	Normal
				mean	59.97	59.97
				stdev	5.73	5.73
				min	25.60	25.60
				max	94.34	94.34
$\sigma_{0,tot,-1}$	Total hoop stress at penetration ID above weld, downhill	Finite element analyses of operational stresses on CRDM nozzle; across various penetration angles	ksi	type	Normal	Normal
				mean	43.18	43.18
				stdev	8.30	8.30
				min	0.00	0.00
				max	92.95	92.95
$\sigma_{0,tot,-2}$	Total hoop stress at penetration OD below weld, downhill	Finite element analyses of operational stresses on CRDM nozzle; across various penetration angles	ksi	type	Normal	Normal
				mean	67.08	67.08
				stdev	10.60	10.60
				min	3.47	3.47
				max	130.69	130.69
$\sigma_{0,tot,-3}$	Total hoop stress at weld surface center, downhill	Finite element analyses of operational stresses on CRDM nozzle; across various penetration angles	ksi	type	Normal	Normal
				mean	61.78	61.78
				stdev	5.77	5.77
				min	27.15	27.15
				max	96.42	96.42

Table B-3
Summary of Loading Inputs for RPVHPN Model (Continued)

Symbol	Description	Source	Units	Parameter Type	Hot Head Base Case	Cold Head Base Case
$R_{1,tot,1}$	Stress gradient quantifier at penetration ID above weld, uphill	Finite element analyses of J–groove weld residual stresses (14 independent analyses)	-	type	Normal	Normal
				mean	1.11	1.11
				stdev	0.24	0.24
				min	0.00	0.00
				max	2.55	2.55
$R_{1,tot,2}$	Stress gradient quantifier at penetration OD below weld, uphill	Finite element analyses of J–groove weld residual stresses (14 independent analyses)	-	type	Normal	Normal
				mean	0.84	0.84
				stdev	0.14	0.14
				min	0.00	0.00
				max	1.68	1.68
$R_{1,tot,3}$	Stress gradient quantifier at weld surface center, uphill	Finite element analyses of J–groove weld residual stresses (14 independent analyses)	-	type	Normal	Normal
				mean	0.89	0.89
				stdev	0.32	0.32
				min	0.00	0.00
				max	2.81	2.81
$R_{1,tot,-1}$	Stress gradient quantifier at penetration ID above weld, downhill	Finite element analyses of J–groove weld residual stresses (14 independent analyses)	-	type	Normal	Normal
				mean	0.60	0.60
				stdev	0.41	0.41
				min	0.00	0.00
				max	3.06	3.06
$R_{1,tot,-2}$	Stress gradient quantifier at penetration OD below weld, downhill	Finite element analyses of J–groove weld residual stresses (14 independent analyses)	-	type	Normal	Normal
				mean	0.51	0.51
				stdev	0.13	0.13
				min	0.00	0.00
				max	1.29	1.29
$R_{1,tot,-3}$	Stress profile curvature quantifier at weld surface center, downhill	Finite element analyses of J–groove weld residual stresses (14 independent analyses)	-	type	Normal	Normal
				mean	0.36	0.36
				stdev	0.17	0.17
				min	0.00	0.00
				max	1.38	1.38

Table B-3
Summary of Loading Inputs for RPVHPN Model (Continued)

Symbol	Description	Source	Units	Parameter Type	Hot Head Base Case	Cold Head Base Case
$R_{0.5,tot,1}$	Stress profile curvature quantifier at penetration ID above weld, uphill	Finite element analyses of J–groove weld residual stresses (14 independent analyses)	-	type	Normal	Normal
				mean	1.08	1.08
				stdev	0.09	0.09
				min	0.54	0.54
				max	1.62	1.62
$R_{0.5,tot,2}$	Stress profile curvature quantifier at penetration OD below weld, uphill	Finite element analyses of J–groove weld residual stresses (14 independent analyses)	-	type	Normal	Normal
				mean	0.87	0.87
				stdev	0.13	0.13
				min	0.09	0.09
				max	1.65	1.65
$R_{0.5,tot,3}$	Stress profile curvature quantifier at weld surface center, uphill	Finite element analyses of J–groove weld residual stresses (14 independent analyses)	-	type	Normal	Normal
				mean	1.21	1.21
				stdev	0.12	0.12
				min	0.49	0.49
				max	1.93	1.93
$R_{0.5,tot,-1}$	Stress profile curvature quantifier at penetration ID above weld, downhill	Finite element analyses of J–groove weld residual stresses (14 independent analyses)	-	type	Normal	Normal
				mean	1.46	1.46
				stdev	0.13	0.13
				min	0.68	0.68
				max	2.24	2.24
$R_{0.5,tot,-2}$	Stress profile curvature quantifier at penetration OD below weld, downhill	Finite element analyses of J–groove weld residual stresses (14 independent analyses)	-	type	Normal	Normal
				mean	0.78	0.78
				stdev	0.09	0.09
				min	0.24	0.24
				max	1.32	1.32
$R_{0.5,tot,-3}$	Stress profile curvature quantifier at weld surface center, downhill	Finite element analyses of J–groove weld residual stresses (14 independent analyses)	-	type	Normal	Normal
				mean	1.47	1.47
				stdev	0.19	0.19
				min	0.33	0.33
				max	2.61	2.61

Table B-4
Summary of Peening-Specific Inputs

Symbol	Description	Source	Units	Parameter Type	Hot Head Base Case	Cold Head Base Case
	Outage of peening application	Scheduled at next outage coinciding with a UT inspection	Cycle number		17	12
	Number of cycles between peening application and final follow-up inspection	Attachment 2	# cycles		2	2
	Inspection interval after peening	Attachment 2	# cycles		5	5
	Interval for BMV post-peening (in number of cycles)	Attachment 2	# cycles		0	3
	Flag indicating if a UT pre-peening exam is performed	Attachment 2	-		TRUE	TRUE
	Flag indicating if a UT exam is included during all the cycle(s) between peening and the follow up exam	Attachment 2	-		TRUE	FALSE
	Flag indicating if BMV exams are performed after peening	Attachment 2	-		TRUE	TRUE
	Number of consecutive cycles in which BMV exams are performed after peening	Attachment 2	# cycles		Perform BMV post-peening per Attachment 2	2

Table B-4
Summary of Peening-Specific Inputs (Continued)

Symbol	Description	Source	Units	Parameter Type	Hot Head Base Case	Cold Head Base Case
$\sigma_{0,PPRS,ID}$ ($t=0$)	Sum of post-peening residual plus normal operating stress on ID surface	Minimum bounding value from performance criteria (Attachment 2)	ksi		10.0	10.0
$x_{1,PPRS,ID}$	Depth of compressive residual stress layer from ID surface	Minimum bounding value from performance criteria (Attachment 2)	in.	type	Normal	Normal
				mean	0.010	0.010
				stdev	0.002	0.002
				min	0.000	0.000
				max	0.025	0.025
$\sigma_{0,PPRS,ext}$ ($t=0$)	Sum of post-peening residual plus normal operating stress on OD and weld surface	Minimum bounding value from performance criteria (Attachment 2)	ksi	mean	10.0	10.0
$x_{1,PPRS,ext}$	Depth of compressive residual stress layer from OD and weld surface	Minimum bounding value from performance criteria (Attachment 2)	in.	type	Normal	Normal
				mean	0.039	0.039
				stdev	0.010	0.010
				min	0.000	0.000
				max	0.098	0.098
$f_{1,PPRS}$	Ratio of minimally-affected depth to penetration depth	See MRP-335 Rev. 1 Section A.3.3	-		2.0	2.0
$f_{2,PPRS}$	Fraction of depth between penetration depth and minimally-affected depth where peening results in no effect	See MRP-335 Rev. 1 Section A.3.3	-		0.7	0.7
	Empirical stress relaxation exponent	Unused in base case, sensitivity case using best-fit value; See MRP-335 Rev. 1 Section A.9.3	-		0.0	0.0

Table B-5
Summary of Inputs for RPVHPN Initiation Model

Symbol	Description	Source	Units	Parameter Type	Hot Head Base Case	Cold Head Base Case
t_1	Time at which failure fraction F_1 is reached on RPVHPNs	Flaw initiation data assessed in MRP–395	EDY		23.0	23.0
σ_c	Standard error in intercept of linearized Weibull fit	Linearized Weibull fit to flaw initiation data assessed in MRP–395	ln(EDY)		0.2705	0.2705
F_1	Arbitrary failure fraction selected to define Weibull PWSCC initiation function	Selected to reflect t_1 as the Weibull scale parameter (characteristic time)	-		0.6321	0.6321
β	Weibull slope for PWSCC flaw initiation on RPVHPNs	Flaw initiation data assessed in MRP–395	-		1.379	1.379
β_{flaw}	Weibull slope for PWSCC multiple flaw initiation on RPVHPNs	Based on representative value for formation of PWSCC at multiple locations in industry SGs	-	type	Normal	Normal
				mean	2.0	2.0
				stdev	0.5	0.5
				min	1.0	1.0
				max	5.0	5.0
ρ_{heat}	Correlation coefficient for PWSCC initiation and propagation of all cracks in Alloy 600	xLPR Input	-		0.0	0.0
ρ_{weld}	Correlation coefficient for PWSCC initiation and propagation of all cracks in Alloy 82/182 weld	xLPR Input	-		0.0	0.0

Table B-5
Summary of Inputs for RPVHPN Initiation Model (Continued)

Symbol	Description	Source	Units	Parameter Type	Hot Head Base Case	Cold Head Base Case
Q_i	Thermal activation energy for PWSCC flaw initiation	Distribution based on laboratory data and experience with Weibull analysis	kcal/mole	type	Normal	Normal
				mean	44.03	44.03
				stdev	3.06	3.06
				min	25.65	25.65
				max	62.41	62.41
$T_{ref,i}$	Reference temperature to normalize PWSCC flaw initiation data	Temperature used to adjust flaw initiation data assessed in this report	°R		1060	1060
a_0	Initial depth assigned to newly initiated flaw	Consistency with initial through-wall fractions of DM weld model	in.	type	Log-Normal	Log-Normal
				linear μ	3.32E-02	3.32E-02
				median	3.12E-02	3.12E-02
				log-norm μ	-3.47	-3.47
				log-norm σ	0.35	0.35
				min	0.02	0.02
				max	0.62	0.62
AR	General initial aspect ratio assigned to newly initiated flaw	Based on aspect ratios of PWSCC cracks observed in inspections of DMW and RPVHPN components	-	type	Log-Normal	Log-Normal
				linear μ	4.77	4.77
				median	4.50	4.50
				log-norm μ	1.50	1.50
				log-norm σ	0.34	0.34
				min	0.57	0.57
				max	35.20	35.20
	Distance from weld toe to location where welding residual stress is equal to 80% of yield stress, uphill side	Finite element analyses of J–groove weld residual stresses; across various units and penetration geometries	in.	type	Normal	Normal
				mean	0.25	0.25
				stdev	0.13	0.13
				min	0.00	0.00
				max	1.03	1.03
	Distance from weld toe to location where welding residual stress is equal to 80% of yield stress, downhill side	Finite element analyses of J–groove weld residual stresses; across various units and penetration geometries	in.	type	Normal	Normal
				mean	0.24	0.24
				stdev	0.06	0.06
				min	0.00	0.00
				max	0.61	0.61

Table B-6
Summary of Inputs for RPVHPN Flaw Propagation Model

Symbol	Description	Source	Units	Parameter Type	Hot Head Base Case	Cold Head Base Case
$1/\Delta t$	Number of time steps per year for crack size increment	The value chosen provides sufficient convergence	1/yr		12	12
f_{heat}	Heat-to-heat factor: common factor applied to all specimens fabricated from the same material to account for manufacturing variations	Fit to heat-to-heat variation data from MRP-55	-	type	Log-normal	Log-Normal
				linear μ	1.68	1.68
				median	1.00	1.00
				75%ile	1.98	1.98
				log-norm μ	0.00	0.00
				log-norm σ	1.02	1.02
				min	0.14	0.14
				max	5.32	5.32
f_{wh}	Within-heat factor: factor accounting for the variability in crack growth rate for different specimens fabricated from the same raw material	Fit to within-heat variation from MRP-55 data after normalizing for heat-to-heat variation factor	-	type	Log-Normal	Log-Normal
				linear μ	1.18	1.18
				median	1.00	1.00
				log-norm μ	0.00	0.00
				log-norm σ	0.57	0.57
				min	0.21	0.21
				max	3.68	3.68
f_{weld}	Weld-to-weld factor: common factor applied to all specimens fabricated from the same weld to account for weld wire/stick heat processing and for weld fabrication	Fit to weld-to-weld variation data from MRP-115	-	type	Log-Normal	Log-Normal
				linear μ	1.19	1.19
				median	1.00	1.00
				75%ile	1.49	1.49
				log-norm μ	0.00	0.00
				log-norm σ	0.589	0.589
				min	0.313	0.313
				max	2.64	2.64
f_{ww}	Within-weld factor: factor accounting for the variability in crack growth rate for different specimens fabricated from the same weld	Fit to within-weld variation from MRP-115 data after normalizing for weld-to-weld variation factor	-	type	Log-Normal	Log-Normal
				linear μ	1.12	1.12
				median	1.00	1.00
				log-norm μ	0.00	0.00
				log-norm σ	0.481	0.481
				min	0.309	0.309
				max	3.24	3.24

Table B-6
Summary of Inputs for RPVHPN Flaw Propagation Model (Continued)

Symbol	Description	Source	Units	Parameter Type	Hot Head Base Case	Cold Head Base Case
α_{heat}	Flaw propagation rate equation power law constant for Alloy 600	Fit to MRP-55 data with power law constant of 1.6 and stress intensity factor threshold of zero	(in/hr)/(ksi-in.$^{0.5}$)$^{1.6}$		3.25E-08	3.25E-08
α_{weld}	Flaw propagation rate equation power law constant for Alloy 182 weld	MRP-115	(in/hr)/(ksi-in.$^{0.5}$)$^{1.6}$		1.62E-07	1.62E-07
Q_g	Thermal activation energy for PWSCC flaw propagation	MRP-115	kcal/mole	type	Normal	Normal
				mean	31.07	31.07
				stdev	1.20	1.20
				min	23.90	23.90
				max	38.24	38.24
$T_{ref,g}$	Absolute reference temperature to normalize PWSCC flaw propagation data	MRP-55, MRP-115	°R		1077	1077
$K_{I,th,heat}$	Flaw propagation rate equation power law threshold for Alloy 600	Conservatively assumed threshold such that all cracks with positive K_I have a non-zero crack growth rate	ksi-sqrt(in.)		0.0	0.0
$K_{I,th,weld}$	Flaw propagation rate equation power law threshold for Alloy 82/182 weld	MRP-115	ksi-sqrt(in.)		0.0	0.0
$K_{I,min,heat}$	Minimum allowable K_I value for Alloy 600 components	No technical basis for non-zero value	ksi-sqrt(in.)		0.0	0.0
$K_{I,min,weld}$	Minimum allowable K_I value for Alloy 182 components	No technical basis for non-zero value	ksi-sqrt(in.)		0.0	0.0
n_{heat}	Flaw propagation rate equation power law exponent for Alloy 600	Fit to MRP-55 data with stress intensity factor threshold of zero	-		1.6	1.6
n_{weld}	Flaw propagation rate equation power law exponent for Alloy 182 weld	MRP-115	-		1.6	1.6
	Flag indicating if crack growth will be predicted considering the effect of crack closure	Crack closure effects are neglected for base case	Logical		FALSE	FALSE
	Flag indicating if cracks may grow in length without the effect of peening stresses	Approximates sub-surface balloon growth of crack	Logical		TRUE	TRUE

Table B-7
Summary of Inputs for RPVHPN Examination Model

Symbol	Description	Source	Units	Parameter Type	Hot Head Base Case	Cold Head Base Case
	The through-wall fraction below which the small-flaw contingency (POD = 0) is used	Smallest flaw size used in UT mockup testing	-		0.10	0.10
$\rho_{insp,UT}$	Correlation coefficient for successive UT inspections	Conservative assumption	-		0.50	0.50
$(a/t_{U,1,UT}, p_{U,1,UT})$	First defined coordinate for favorable UT POD curve	Conservative assumption relative to UT qualification criteria	-		(0.2,0.80)	(0.2,0.80)
$(a/t_{U,2,UT}, p_{U,2,UT})$	Second defined coordinate for favorable UT POD curve	Conservative assumption relative to UT qualification criteria	-		(0.4,0.95)	(0.4,0.95)
$(a/t_{L,1,UT}, p_{L,1,UT})$	First defined coordinate for unfavorable UT POD curve	Conservative assumption relative to UT qualification criteria	-		(0.4,0.65)	(0.4,0.65)
$(a/t_{L,2,UT}, p_{L,2,UT})$	Second defined coordinate for unfavorable UT POD curve	Conservative assumption relative to UT qualification criteria	-		(0.7,0.90)	(0.7,0.90)
	Stdev between mean UT POD curve and favorable/unfavorable curves	Conservative assumption relative to UT qualification criteria	-		2	2
$p_{max,UT}$	Maximum probability of detection for UT inspection	Conservative assumption relative to UT qualification criteria	-		0.95	0.95
p_{BMV}	Probability of detection for visual inspection of leaking nozzle	Conservative assumption	-		0.90	0.90
$\rho_{insp,BMV}$	Correlation coefficient for successive BMV inspections	Conservative assumption	-		0.95	0.95

Table B-8
Summary of Inputs for RPVHPN Stability Model

Symbol	Description	Source	Units	Parameter Type	Hot Head Base Case	Cold Head Base Case
$\theta_{circ,init}$	Initial angle for circumferential through-wall cracks immediately following a leak	MRP-105	degrees		30	30
$\theta_{circ,crit}$	Critical flaw angle for nozzle ejection	MRP-110	degrees		300	300
$K_{circ,mult}$	Circumferential through-wall crack K_I curve multiplier	Assumed to assure conservative application of FEA-predicted K_I curves	-	type	triangular	triangular
				mode	1	1
				lower limit	1	1
				upper limit	2	2
$c_{circ,mult}$	Circumferential through-wall crack environmental factor	Conservative factor applied based on anecdotal information about environment effects on circumferential TW cracks	-	type	triangular	triangular
				mode	1	1
				lower limit	1	1
				upper limit	2	2

B.2.2 Probabilistic Sensitivity Studies

Sensitivity studies are performed with respect to various model parameters to characterize the impact of modeling assumptions and input uncertainty on nozzle leakage and ejection risk predictions. The results of these sensitivity studies are presented in Section B.3.3.

Table B-9 and Table B-10 list the values of the parameters that are varied in each sensitivity study. For each case, all parameters not included in the table remain identical to the base case inputs listed in Table B-1 through Table B-8. Studies listed in Table B-9 are classified as an Inspection Scheduling Sensitivity (in which a controllable inspection scheduling option is varied) and Table B-10 lists Model Sensitivity Cases (in which a modeling input or characteristic is varied).

Table B-9
Summary of Modified Inputs for RPVHPN Inspection Scheduling Sensitivity Cases

Sensitivity Case	Description	Symbol	Units	Parameter Type	Hot Base Case Value	Hot Sensitivity Case Value	Cold Base Case Value	Cold Sensitivity Case Value
S1	Skip follow-up UT inspection and enter post peening ISI schedule		-		Perform follow-up UT 1st and 2nd cycle after peening	Skip follow-up UT inspection; first ISI after 5 cycles	Perform follow-up UT 2nd cycle after peening	Skip follow-up UT inspection; first ISI after 5 cycles
S2	Skip UT during pre-peening inspection		-		Perform UT during pre-peening inspection	Skip UT during pre-peening inspection	Perform UT during pre-peening inspection	Skip UT during pre-peening inspection
S3	BMV every other cycle post-peening		-		Perform BMV post-peening per Attachment 2	Perform BMV every 2nd outage post-peening	Perform BMV post-peening per Attachment 2	Perform BMV every 2nd outage post-peening
S4	BMV every third cycle post-peening		-		Perform BMV post-peening per Attachment 2	Perform BMV every 3rd outage post-peening		
S5	Do not perform BMV after peening		-		Perform BMV post-peening per Attachment 2	Do not perform BMV after peening	Perform BMV post-peening per Attachment 2	Do not perform BMV after peening
S6	Do not perform UT during all cycles between peening and follow-up exam		-		Perform follow-up UT 1st and 2nd cycle after peening	Perform follow-up UT 2nd cycle after peening		

Table B-10
Summary of Modified Inputs for RPVHPN Model Sensitivity Cases

Sensitivity Case	Description	Symbol	Units	Parameter Type	Hot Base Case Value	Hot Sensitivity Case Value	Cold Base Case Value	Cold Sensitivity Case Value
M1	Reduce operating capacity factor	CF	-		0.97	0.92		
M2	Reject trials with detections/ejections before given cycle (i.e. present day)		Cycle number		0	16	0	11
M3	Increase number of modeled penetrations	N_{pen}	-		78	97		
M4	Decrease nozzle thickness and OD	t	in.		0.62	0.39		
		D_o	in.		4.00	3.50		
M5	Halve growth integration time step	$1/\Delta t$	1/yr		12	24		
M6	Linearly extrapolate POD to zero below 10% TW		-		Assume POD = 0 below 10% TW	Linearly extrapolate		
M7	Remove correlation between UT inspections	$\rho_{insp,UT}$	-		0.50	0.00		
M8	Decrease maximum UT probability of detection to 90%	$p_{max,UT}$	-		0.95	0.90	0.95	0.90
M9	Remove correlation between BMV inspections	$\rho_{insp,BMV}$	-		0.95	0.00	0.95	0.00
M10	Decrease critical flaw angle for nozzle ejection	$\theta_{circ,crit}$	degrees		300	275	300	275

Table B-10
Summary of Modified Inputs for RPVHPN Model Sensitivity Cases (Continued)

Sensitivity Case	Description	Symbol	Units	Parameter Type	Hot Base Case Value	Hot Sensitivity Case Value	Cold Base Case Value	Cold Sensitivity Case Value
M11	Double standard deviation of peening penetration depth	$x_{1,PPRS,ID}$	in.	type	Normal	Normal		
				mean	0.010	0.010		
				stdev	0.002	0.005		
				min	0.000	0.000		
				max	0.025	0.049		
		$x_{1,PPRS,ext}$	in.	type	Normal	Normal		
				mean	0.039	0.039		
				stdev	0.010	0.020		
				min	0.000	0.000		
				max	0.098	0.236		
M12	Increase peening compressive surface stress and penetration depth	$\sigma_{0,PPRS,ID}$ (t=0)	ksi		Normal operating plus residual stress is +10 ksi tensile	Residual stress is 100 ksi compressive		
		$x_{1,PPRS,ID}$	in.	type	Normal	Normal		
				mean	0.010	0.020		
				stdev	0.002	0.005		
				min	0.000	0.000		
				max	0.025	0.049		
		$\sigma_{0,PPRS,ext}$ (t=0)	ksi		Normal operating plus residual stress is +10 ksi tensile	Residual stress is 100 ksi compressive		
		$x_{1,PPRS,ext}$	in.	type	Normal	Normal		
				mean	0.039	0.118		
				stdev	0.010	0.059		
				min	0.000	0.000		
				max	0.098	0.295		
M13	Decrease initiation characteristic time by factor of 5	t_1	EDY		23.0	4.6	23.0	4.6
M14	Increase multiple flaw initiation slope	β_{flaw}	-	type	Normal	Normal	Normal	Normal
				mean	2.0	3.0	2.0	3.0
				stdev	0.5	0.5	0.5	0.5
				min	1.0	2.0	1.0	2.0
				max	5.0	6.0	5.0	6.0

Table B-10
Summary of Modified Inputs for RPVHPN Model Sensitivity Cases (Continued)

Sensitivity Case	Description	Symbol	Units	Parameter Type	Hot Base Case Value	Hot Sensitivity Case Value	Cold Base Case Value	Cold Sensitivity Case Value
M15	Sample multiple flaw initiation slope a single time per head		-		Sample multiple flaw initiation slope once per penetration	Sample multiple flaw initiation slope once per head		
M16	Include initiation-growth correlation	ρ_{heat}	-		0.0	-0.8	0.0	-0.8
		ρ_{weld}	-		0.0	-0.8	0.0	-0.8
M17	Decrease initiation activation energy	Q_i	kcal/mole	type			Normal	Normal
				mean			44.03	40.03
				stdev			3.06	3.06
				min			25.65	21.64
				max			62.41	58.41
M18	Decrease median initial crack depth by factor of 5 and remove minimum, impose minimum K_I value	a_0	in.	type	Log-Normal	Log-Normal	Log-Normal	Log-Normal
				linear μ	0.033	0.006	0.033	0.006
				median	0.031	0.006	0.031	0.006
				log-norm μ	-3.467	-5.127	-3.467	-5.127
				log-norm σ	0.354	0.354	0.354	0.354
				min	0.020	0.000	0.020	0.000
				max	0.622	0.622	0.622	0.622
		$K_{I,min,heat}$	ksi-sqrt(in.)		0.00	10.92	0.00	10.92
		$K_{I,min,weld}$	ksi-sqrt(in.)		0.00	10.92	0.00	10.92
M19	Utilize crack closure methodology and decrease initial flaw depth		-		Do not utilize crack closure	Utilize crack closure	Do not utilize crack closure	Utilize crack closure
		a_0	in.	type	Log-Normal	Log-Normal	Log-Normal	Log-Normal
				linear μ	0.033	0.006	0.033	0.006
				median	0.031	0.006	0.031	0.006
				log-norm μ	-3.467	-5.127	-3.467	-5.127
				log-norm σ	0.354	0.354	0.354	0.354
				min	0.020	0.000	0.020	0.000
				max	0.622	0.622	0.622	0.622
M20	Increase median initial crack depth	a_0	in.	type	Log-Normal	Log-Normal	Log-Normal	Log-Normal
				linear μ	0.033	0.146	0.033	0.146
				median	0.031	0.137	0.031	0.137
				log-norm μ	-3.467	-1.987	-3.467	-1.987
				log-norm σ	0.354	0.354	0.354	0.354
				min	0.020	0.020	0.020	0.020
				max	0.622	0.622	0.622	0.622

Table B-10
Summary of Modified Inputs for RPVHPN Model Sensitivity Cases (Continued)

Sensitivity Case	Description	Symbol	Units	Parameter Type	Hot Base Case Value	Hot Sensitivity Case Value	Cold Base Case Value	Cold Sensitivity Case Value
M21	MRP-55 Crack Growth Rate Model Parameters	α_{heat}	$(in/hr)/(ksi\text{-}in.^{0.5})^{1.6}$		3.25E-08	2.21E-07		
		$K_{1,th,heat}$	ksi-sqrt(in.)		0.00	8.19		
		n_{heat}	-		1.60	1.16		
M22	Decrease growth activation energy	Q_g	kcal/mole	type			Normal	Normal
				mean			31.07	28.68
				stdev			1.20	1.20
				min			23.90	21.51
				max			38.24	35.85
M23	Prevent balloon growth		-		Allow balloon growth	Prevent balloon growth		
M24	Remove crack environmental factor	$c_{circ,mult}$	-	type	triangular	constant	triangular	constant
				mode	1	1	1	1
				lower limit	1	-	1	-
				upper limit	2	-	2	-
M25	Increase peening compressive surface stress and penetration depth, prevent balloon growth, utilize crack closure	$\sigma_{0,PPRS,ID}$ (t=0)	ksi		Normal operating plus residual stress is +10 ksi tensile	Residual stress is 100 ksi compressive		
		$x_{1,PPRS,ID}$	in.	type	Normal	Normal		
				mean	0.010	0.020		
				stdev	0.002	0.005		
				min	0.000	0.000		
				max	0.025	0.049		
		$\sigma_{0,PPRS,ext}$ (t=0)	ksi		Normal operating plus residual stress is +10 ksi tensile	Residual stress is 100 ksi compressive		
		$x_{1,PPRS,ext}$	in.	type	Normal	Normal		
				mean	0.039	0.118		
				stdev	0.010	0.059		
				min	0.000	0.000		
				max	0.098	0.295		
			-		Do not utilize crack closure	Utilize crack closure		
			-		Allow balloon growth	Prevent balloon growth		

B.3 Probabilistic Model Results

B.3.1 Preliminaries

Ejections and leakage are counted in two different ways within the simulation framework: in terms of the number of heads with at least one event (by counting only the first instance of leakage or ejection for a given MC realization) and in terms of the number of penetrations with at least one event (by counting the first instance of leakage or the occurrence of ejection for each unique penetration). The primary ejection and leakage statistics used to assess and compare the results of the probabilistic model are defined below:

- Incremental leakage frequency (ILF) is defined as the average number of new leaking nozzles per year on a RPV top head. A simulated flaw causes leakage if it propagates through the entire material thickness to penetrate the annulus above the J-groove weld before it is detected and repaired. This statistic is derived for any given operational cycle by averaging the predicted number of new leaking nozzles for that operational cycle across all MC realizations. This is adjusted to a probability per year by dividing by the number calendar years per cycle.

$$ILF = \frac{(\text{Number of new leaking nozzles predicted during cycle across all realizations})}{(\text{Number of realizations})(\text{Calendar years per cycle})} \qquad \text{[B-1]}$$

- Average leakage frequency (ALF) is the average of the ILFs following the hypothetical time of peening until the end of the operational service period of the plant.

$$ALF = \frac{\sum_{i=i_{peen}}^{N_{cycle}} (\text{Number of new leaking nozzles predicted during cycle across all realizations})}{(\text{Number of realizations})(\text{Calendar years per cycle})(N_{cycle} - i_{peen})} \qquad \text{[B-2]}$$

where:

N_{cycle} = number of cycles in operational service period
i_{peen} = cycle number associated with the hypothetical time of peening

- Cumulative probability of leakage (CPL) is defined as the fraction of heads with at least one predicted leak across all MC realizations across all cycles of interest. This document reports two versions of this statistic: (1) cumulated from the start of operation to a given cycle and (2) cumulated from the hypothetical time of peening to the end of plant operation.

$$CPL = \frac{(\text{Total number of heads with at least one predicted leak})}{(\text{Number of realizations})} \qquad \text{[B-3]}$$

- Incremental ejection frequency (IEF) is defined as the average number of nozzle ejections per year on a RPV top head. This statistic is derived for any given operational cycle by averaging the predicted number of ejections for that operational cycle across all MC realizations and dividing by the number of calendar years per cycle. If no ejections are

predicted to occur during a given cycle across all MC realizations, 0.5 ejections are assumed for the sake of stability and conservatism in calculated statistic values.

$$IEF = \frac{\max\{(\text{Number of ejections leaks predicted during cycle across all realizations}),0.5\}}{(\text{Number of realizations})(\text{Calendar years per cycle})} \quad \text{[B-4]}$$

- Average ejection frequency (AEF) is the average of the IEFs following the hypothetical time of peening until the end of the operational service period of the plant.

$$AEF = \frac{\sum_{i=i_{peen}}^{N_{cycle}} \max\{(\text{Number of ejections predicted during } i\text{th cycle across all realizations}),0.5\}}{(\text{Number of realizations})(\text{Calendar years per cycle})(N_{cycle} - i_{peen})} \quad \text{[B-5]}$$

- Cumulative probability of ejection (CPE) is defined as the fraction of heads with at least one predicted ejection across all MC realizations across all cycles of interest. This document reports two versions of this statistic: (1) cumulated from the start of operation to a given cycle and (2) cumulated from the hypothetical time of peening to the end of plant operation.

$$CPE = \frac{(\text{Total number of heads with at least one predicted ejection})}{(\text{Number of realizations})} \quad \text{[B-6]}$$

The effect of nozzle ejection on nuclear safety can be assessed through multiplication of the frequency of nozzle ejection (i.e., the initiating event frequency) with appropriate conditional core damage probability (CCDP) value. The resulting core damage frequency is typically averaged over long-term operation and compared to the acceptance criteria of Regulatory Guide 1.174 [10]. Regulatory Guide 1.174 specifies an acceptable change in core damage frequency of 1×10^{-6} per reactor year for permanent changes in plant design parameters, technical specifications, etc.

More vital conclusions are drawn from the relative differences between these statistics predicted for different cases (e.g., between the CPL predicted for one peening schedule vs. the CPL predicted with a different peening schedule). This approach minimizes any potential for bias introduced by the various modeling assumptions.

B.3.2 Base Case Results

The base case probabilistic runs resulted in an average ejection frequency (AEF) of 1.7×10^{-5} for the hot-head base case with peening, which compares to an AEF of 2.1×10^{-5} for the hot-head base case without peening mitigation. This is shown in Figure B-2.

As PWSCC is a thermally activated degradation mechanism, the number of leaks and nozzle ejections for the cold-head cases are expected to be lower than the corresponding hot-head cases. Appropriately, the AEF for the cold-head base case with peening is 1.3×10^{-6}, and the AEF for the cold-head base case without peening mitigation is 1.9×10^{-6}. This is shown in Figure B-3.

For both reactor pressure vessel head temperatures evaluated, the peening base case provides a risk-neutral alternative to the no-peening base case. I.e., the peening base case provides equivalent or reduced risk with respect to the no-peening base case.

Furthermore, the absolute acceptance criterion of an AEF below 5×10^{-5}, which results in an acceptable change in core damage frequency well below 1×10^{-6} per reactor year, is met by all four base cases (hot and cold heads, with and without peening mitigation).

Figure B-4 and Figure B-5 compare time-histories of IEF and CPE for peening and no-peening base cases. Figure B-8, Figure B-9, and Figure B-10 compare time-histories of ILF and CPL for peening and no-peening base cases. Figure B-6 and Figure B-7 indicate that peening reduces the cumulative probability of leakage from the hypothetical time of peening to the end of operational service of the plant approximately by a factor of five.

B.3.3 Sensitivity Study Results

Only three sensitivity cases for the hot-head model exceed the absolute acceptance criterion of an AEF of 5×10^{-5}, all of which feature inspection schedules relaxed beyond those of the base cases (e.g. omitting pre-peening or follow-up examinations). This emphasizes the importance of pre-peening and follow-up inspections, such that pre-existing cracks that extend beyond the peening compressive layer are detected and repaired. All Model Sensitivity cases for the hot-head, as well as all sensitivity cases for the cold-head remain below the absolute acceptance criterion.

Figure B-11 and Figure B-16 compare the average ejection frequencies from the peening inspection scheduling sensitivity cases to those for the peening and non-peening base cases. Figure B-12, Figure B-13, and Figure B-17 compare the AEFs resulting from the model sensitivity cases with peening to those for the peening base case. Figure B-14, Figure B-15, and Figure B-18 compare the AEFs resulting from the model sensitivity cases with no-peening to those for the no-peening base case. Additionally, Figure B-19 provides time-histories for IEF and CPE for Model Sensitivity case M2, which re-samples all MC realizations with at least one detection of cracking prior to the hypothetical time of peening.

The following model sensitivity cases resulted in an increase in the ratio of the average ejection frequency for the peened component relative to the unmitigated component:

- Hot Model Sensitivity Case 13 – Arbitrarily reducing the initiation reference time by a factor of five results in an AEF of 3.3×10^{-5} for the peened component and an AEF of 2.9×10^{-5} for the unmitigated component. The predicted AEF and ALF for this sensitivity case result in the greatest increase with respect to the base case. However, it is noted that this initiation model results in a prediction of leakage before 20 EFPY in over 95% of hot reactor heads. This is not in line with U.S. PWR operating experience.
- Hot Model Sensitivity Case 18 – Applying a smaller initial flaw size and enforcing a minimum allowable stress intensity factor results in an AEF of 2.9×10^{-5} for the peened component and an AEF of 2.0×10^{-5} for the unmitigated component. However, there is no technical basis for applying a nonzero minimum allowable stress intensity factor.
- Hot Model Sensitivity Case 19 – Applying a smaller initial flaw size and utilizing crack closure results in an AEF of 2.6×10^{-5} for the peened component and an AEF of 2.2×10^{-5} for the unmitigated component. However, the reduced initial flaw size provides most of this effect. Smaller flaw sizes are expected to lead to a relative increase in risk, as they are less likely to be detected in pre-peening and follow-up examinations. This results in an increased number of active cracks during the post-peening ISI schedule.

- Hot Model Sensitivity Case 21 – Applying the MRP-55 CGR Model results in an AEF of 1.6×10^{-5} for the peened component and an AEF of 1.4×10^{-5} for the unmitigated component. The predicted AEF for this sensitivity case is less than that of the corresponding base case values.
- Hot Model Sensitivity Case 24 – Removing the circumferential crack environmental factor results in an AEF of 8.4×10^{-6} for the peened component and an AEF of 4.5×10^{-6} for the unmitigated component. The predicted AEF for this sensitivity case is about half of the AEF for the corresponding base case values.
- No Cold Model Sensitivity Cases resulted in an increased AEF for the peened component relative to the unmitigated component.

Furthermore, the average penetration leakage frequencies due to cracks initiating in the nozzle tube base metal remain below 0.05 new leaking penetrations per year for all peening cases evaluated.

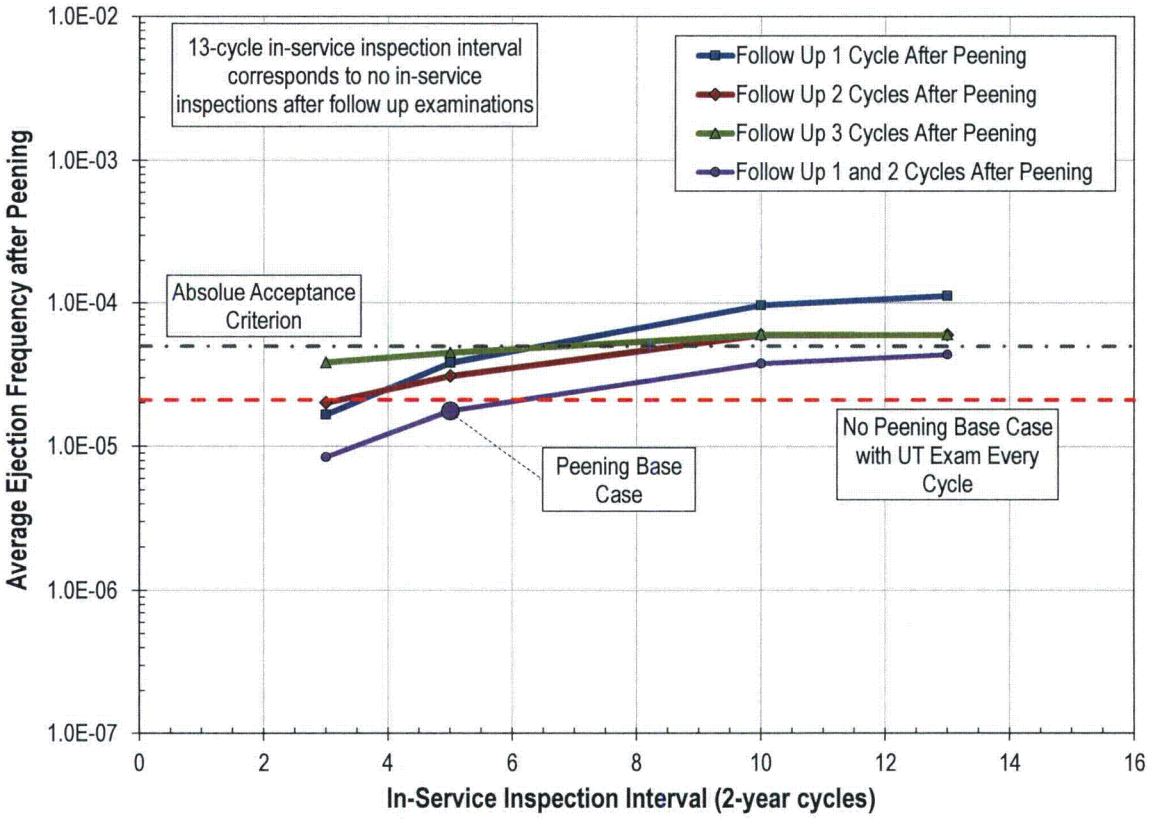

Figure B-2
Average Ejection Frequency from Hypothetical Time of Peening to End of Operational Service Period vs. ISI Frequency for Hot Reactor Head

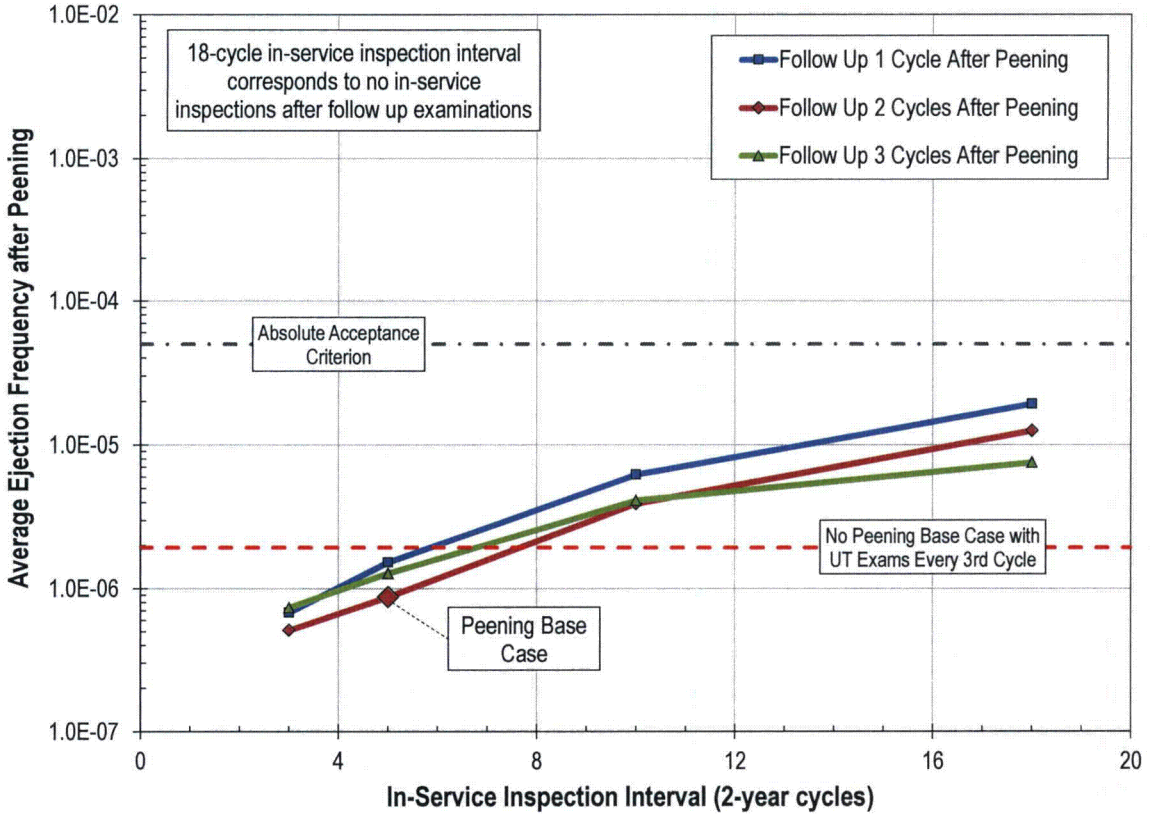

Figure B-3
Average Ejection Frequency from Hypothetical Time of Peening to End of Operational Service Period vs. ISI Frequency for Cold Reactor Head

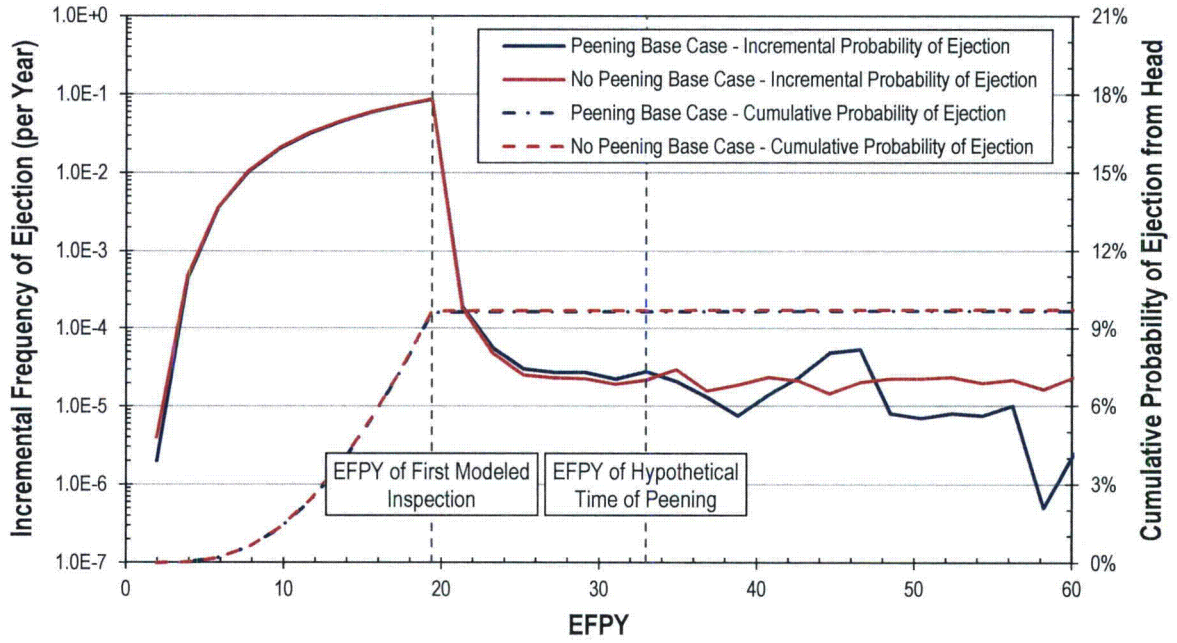

Figure B-4
Prediction of Nozzle Ejection vs. Time for Hot RPVHPNs

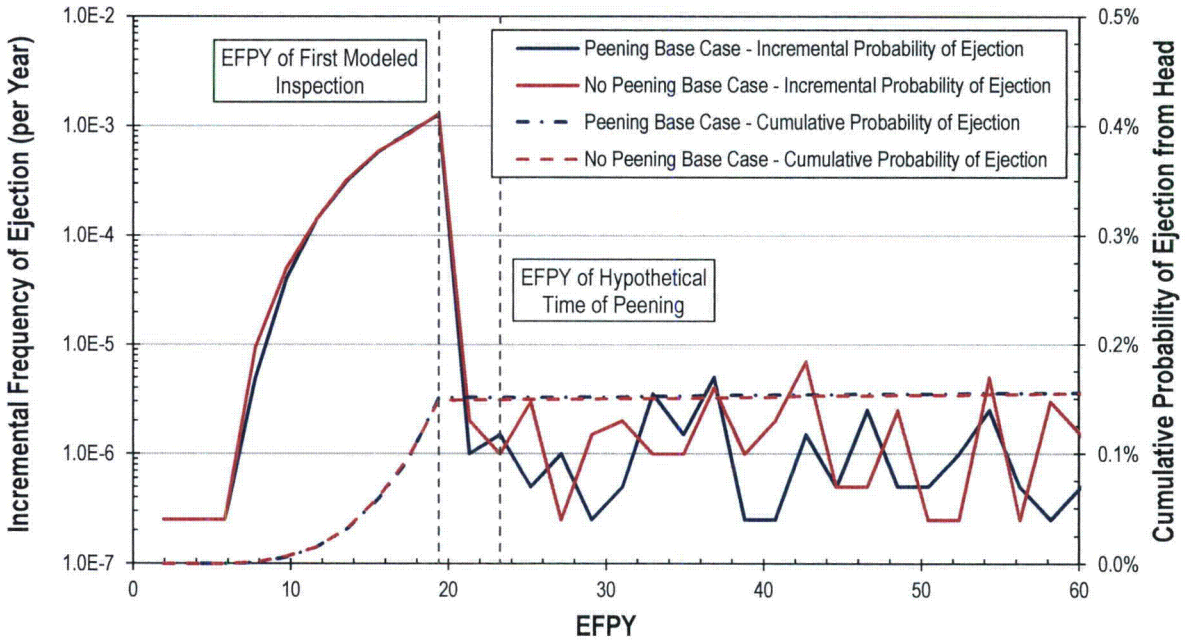

Figure B-5
Prediction of Nozzle Ejection vs. Time for Cold RPVHPNs

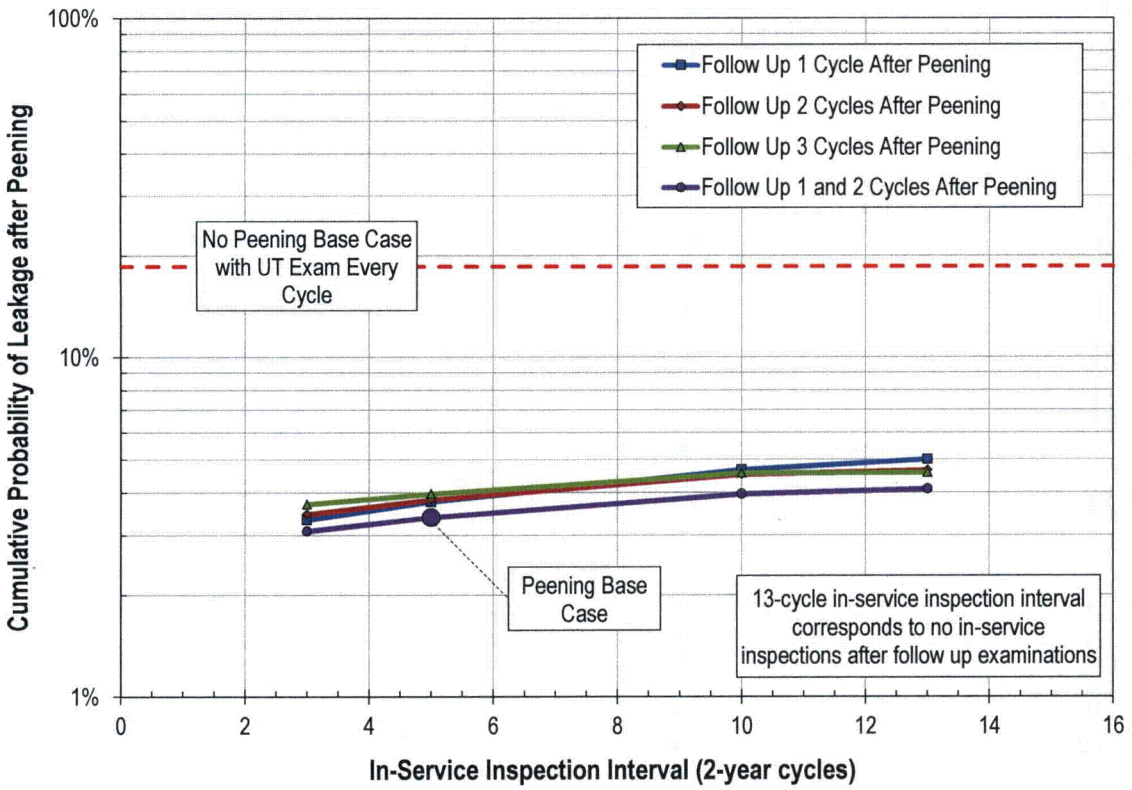

Figure B-6
Cumulative Probability of Leakage from Hypothetical Time of Peening to End of Operational Service Period vs. ISI Frequency for Hot Reactor Head

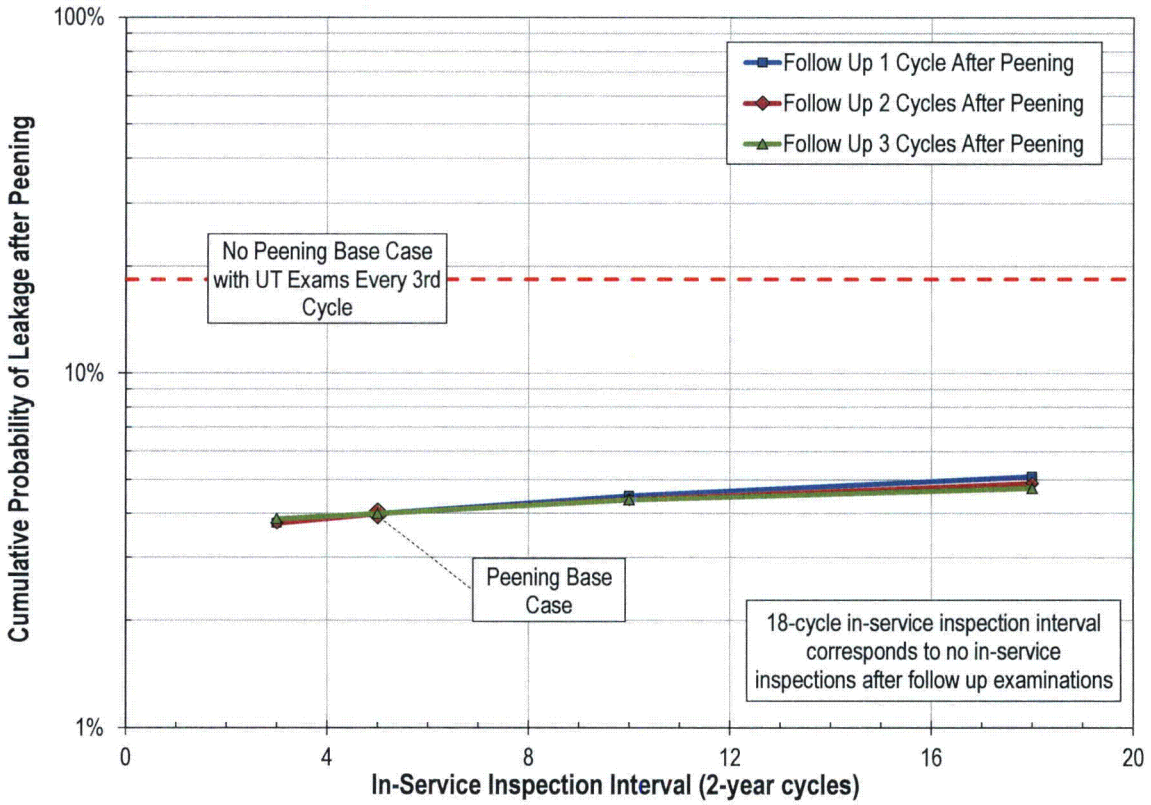

Figure B-7
Cumulative Probability of Leakage from Hypothetical Time of Peening to End of Operational Service Period vs. ISI Frequency for Cold Reactor Head

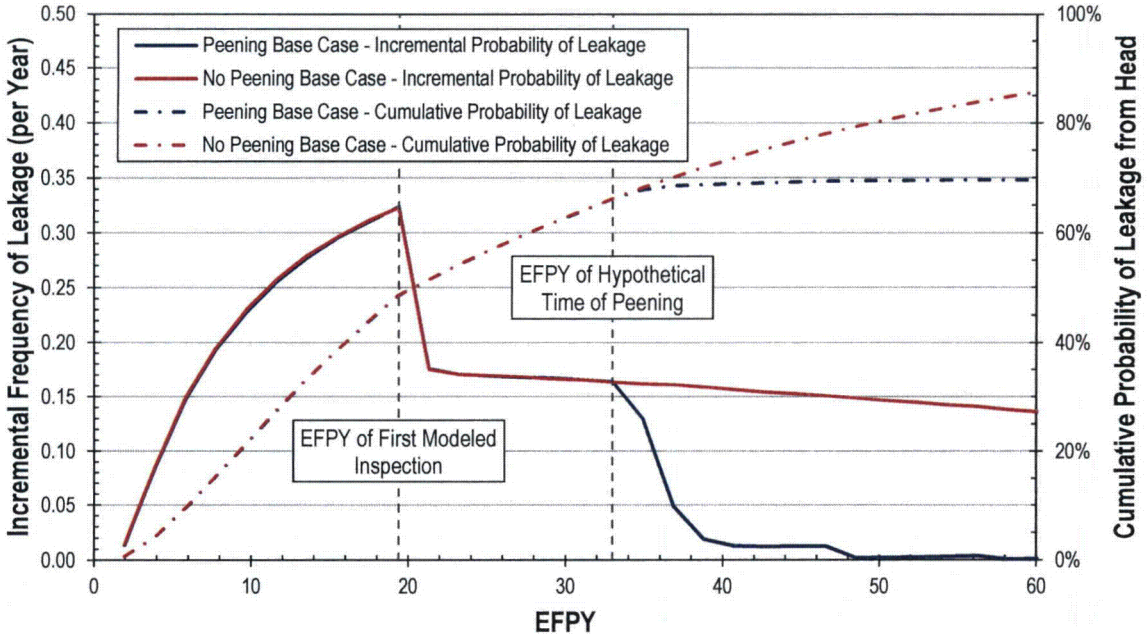

Figure B-8
Prediction of Leakage vs. Time for Hot RPVHPNs

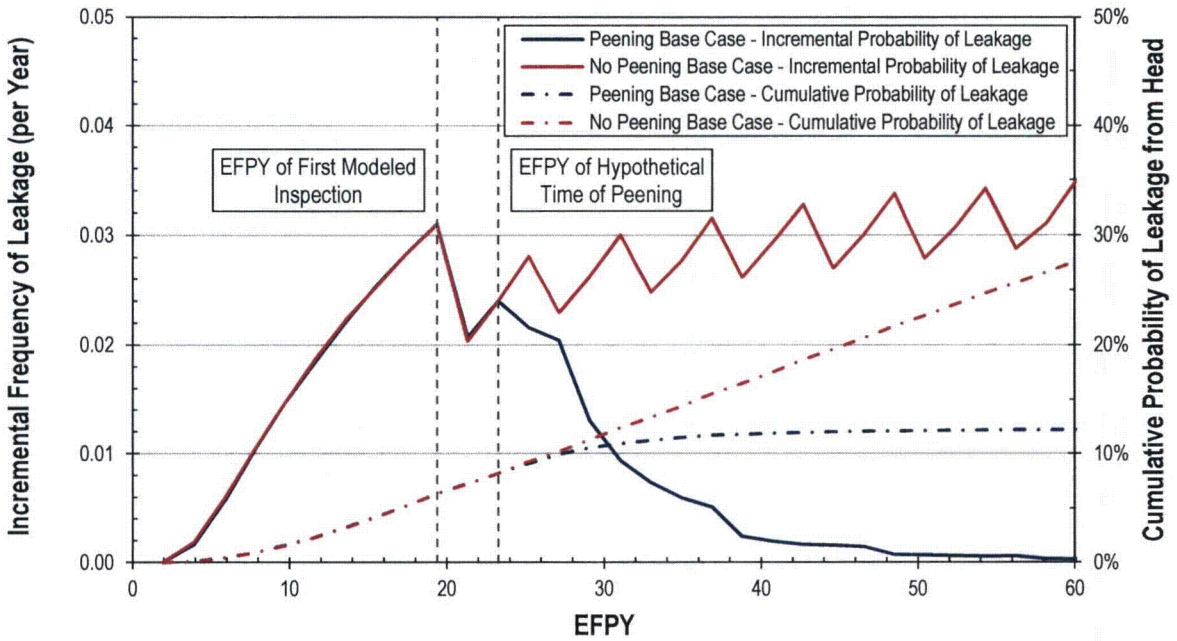

Figure B-9
Prediction of Leakage vs. Time for Cold RPVHPNs

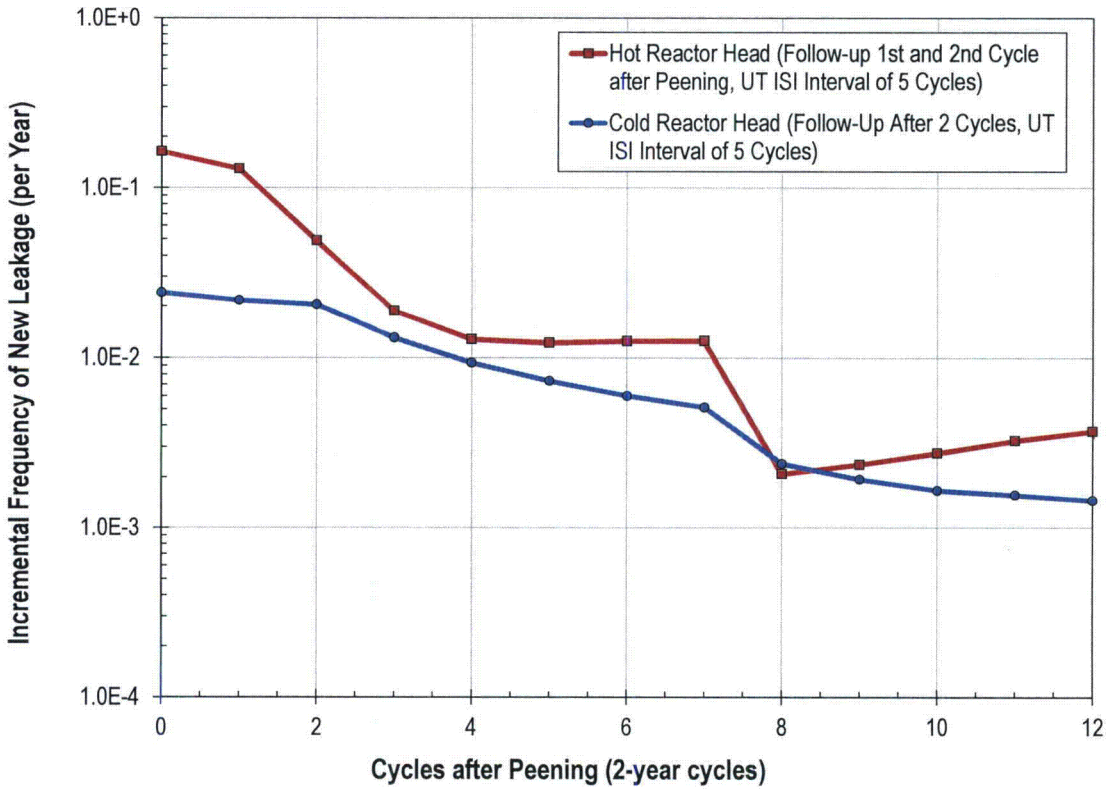

Figure B-10
Incremental Frequency of Leakage after Peening with Relaxed ISI Intervals

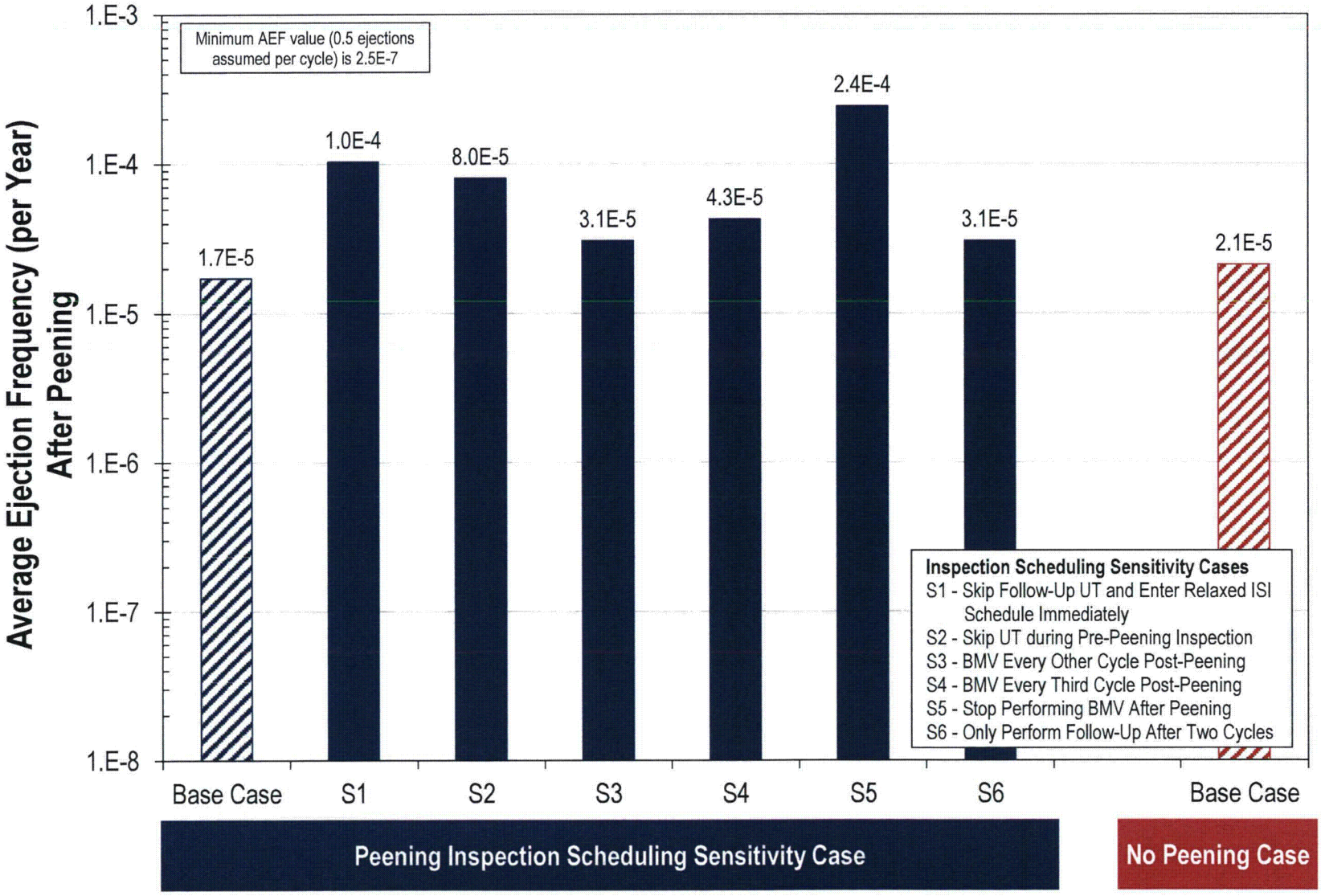

Figure B-11
Summary for Inspection Scheduling Sensitivity Results for Hot RPVHPN Probabilistic Model with Peening

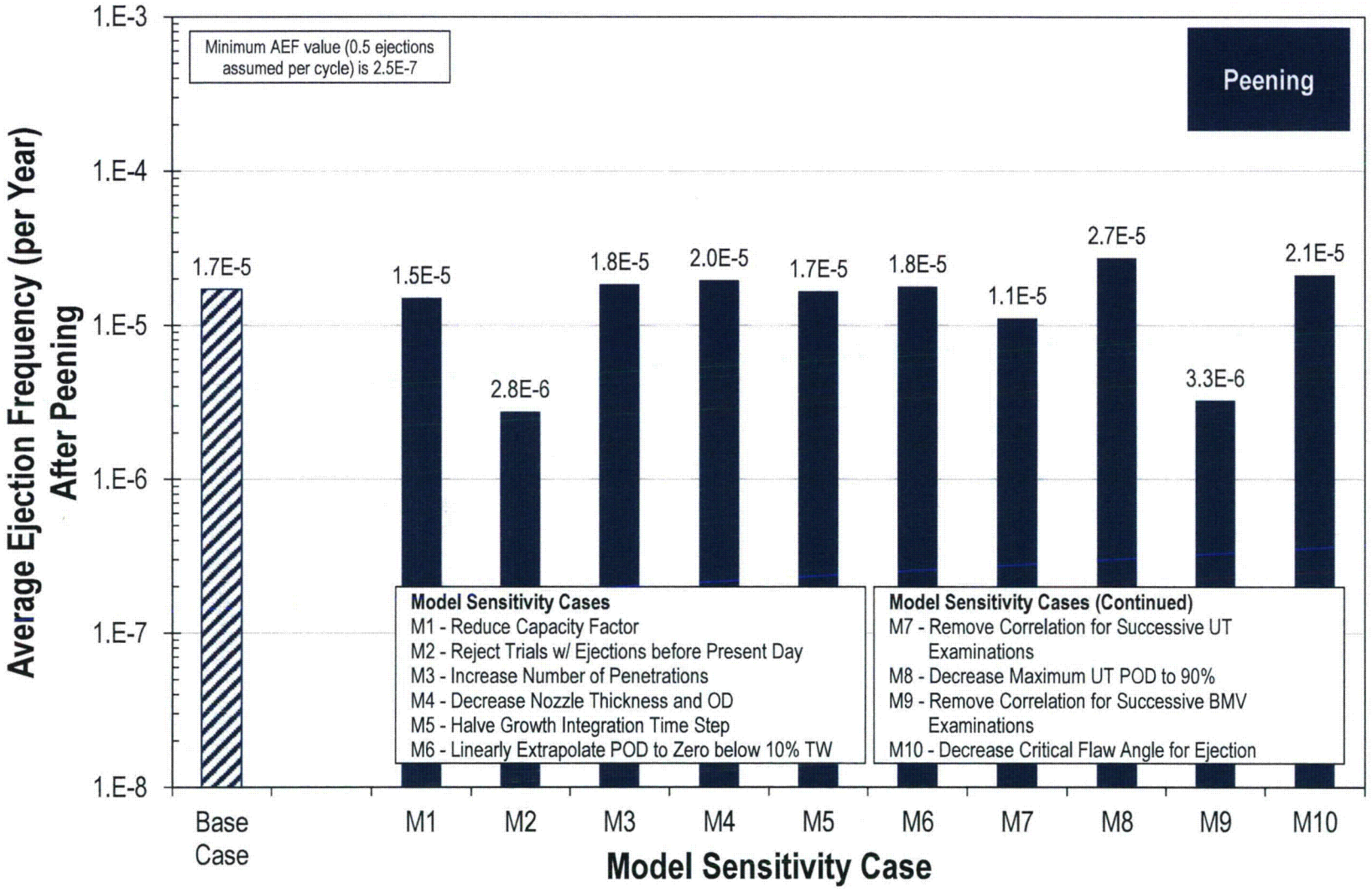

Figure B-12
Summary of Model Sensitivity Results for Hot RPVHPN Probabilistic Model with Peening

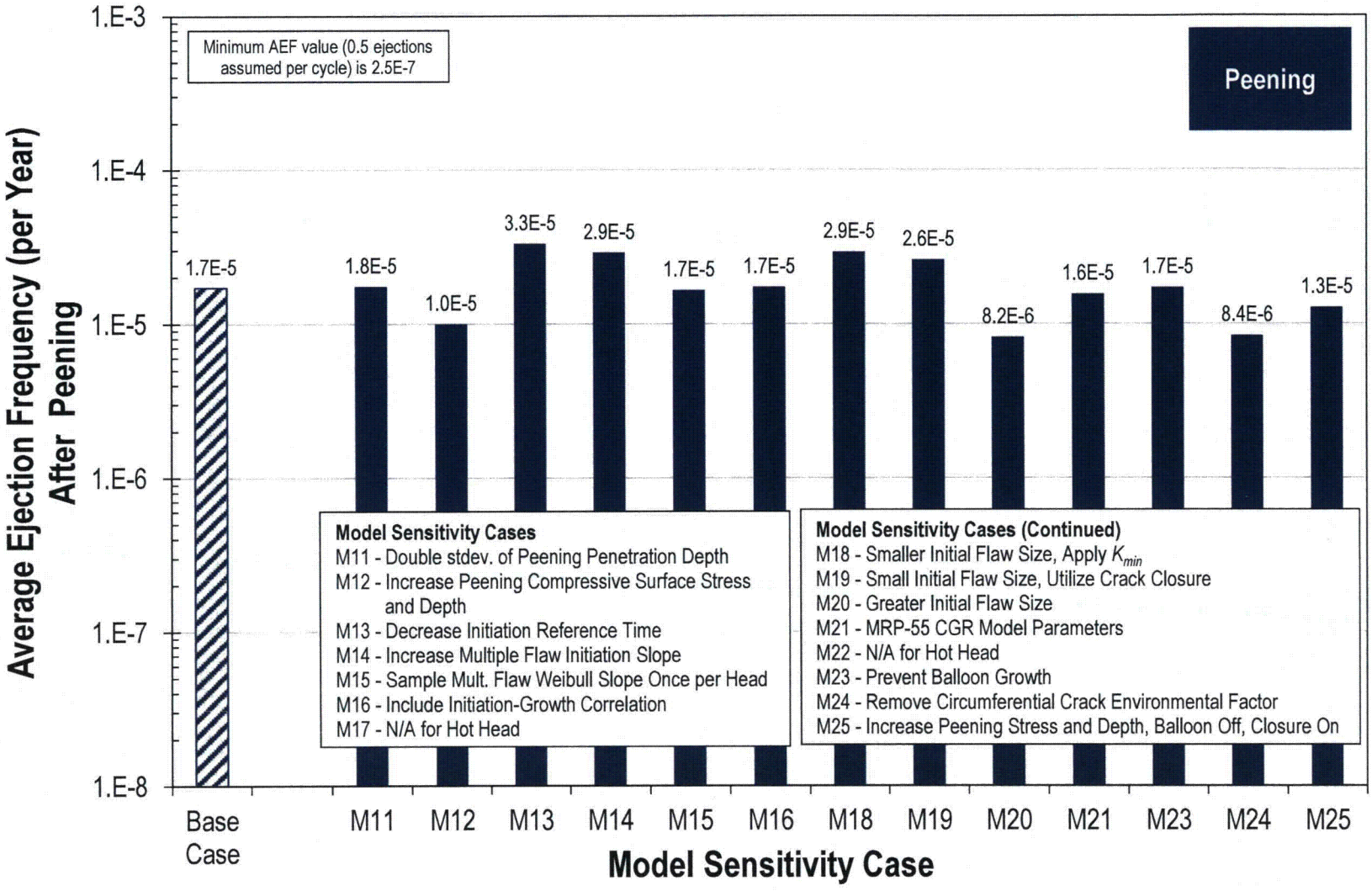

Figure B-13
Summary of Model Sensitivity Results for Hot RPVHPN Probabilistic Model with Peening (Continued)

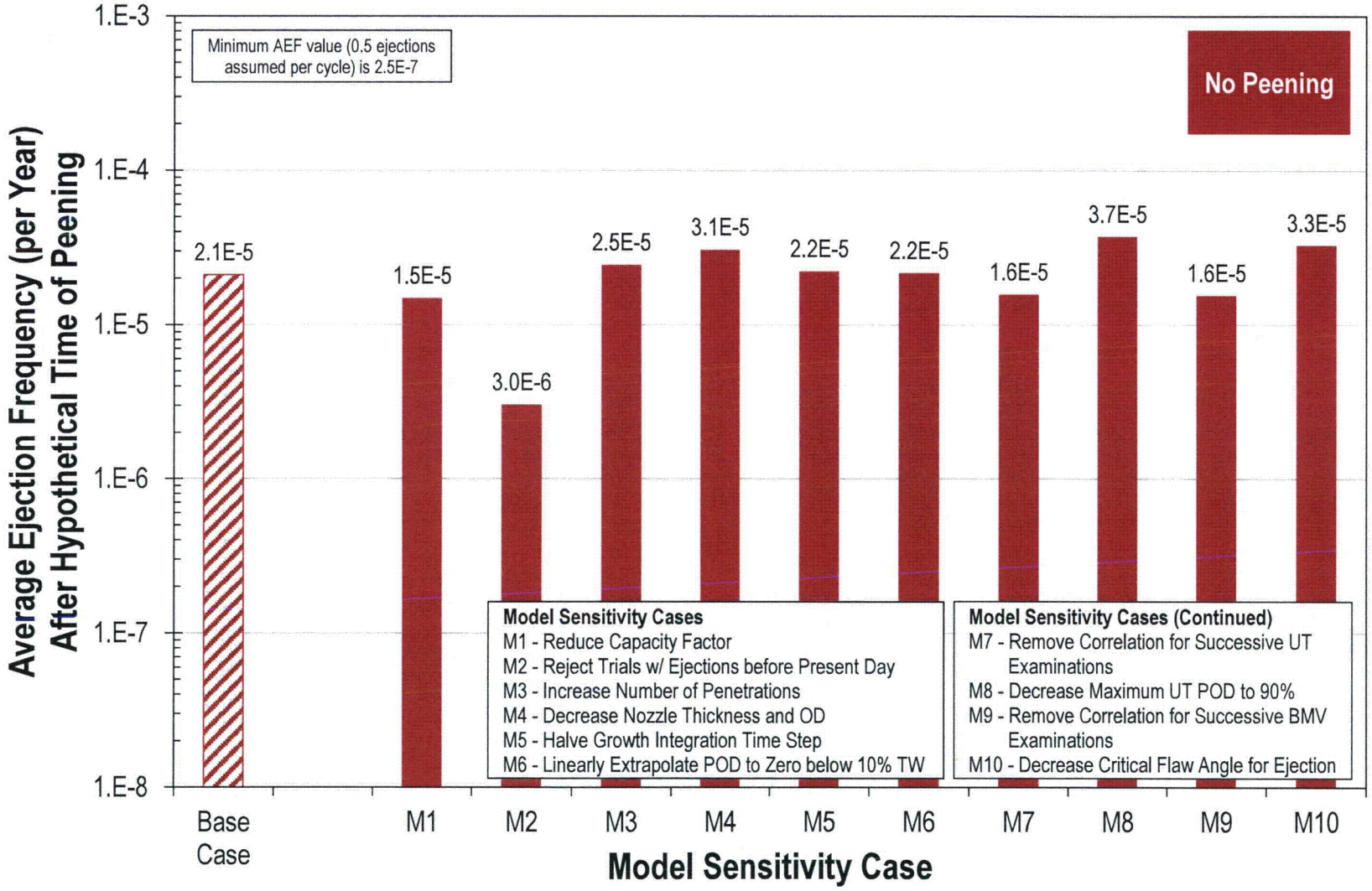

Figure B-14
Summary of Model Sensitivity Results for Hot RPVHPN Probabilistic Model without Peening

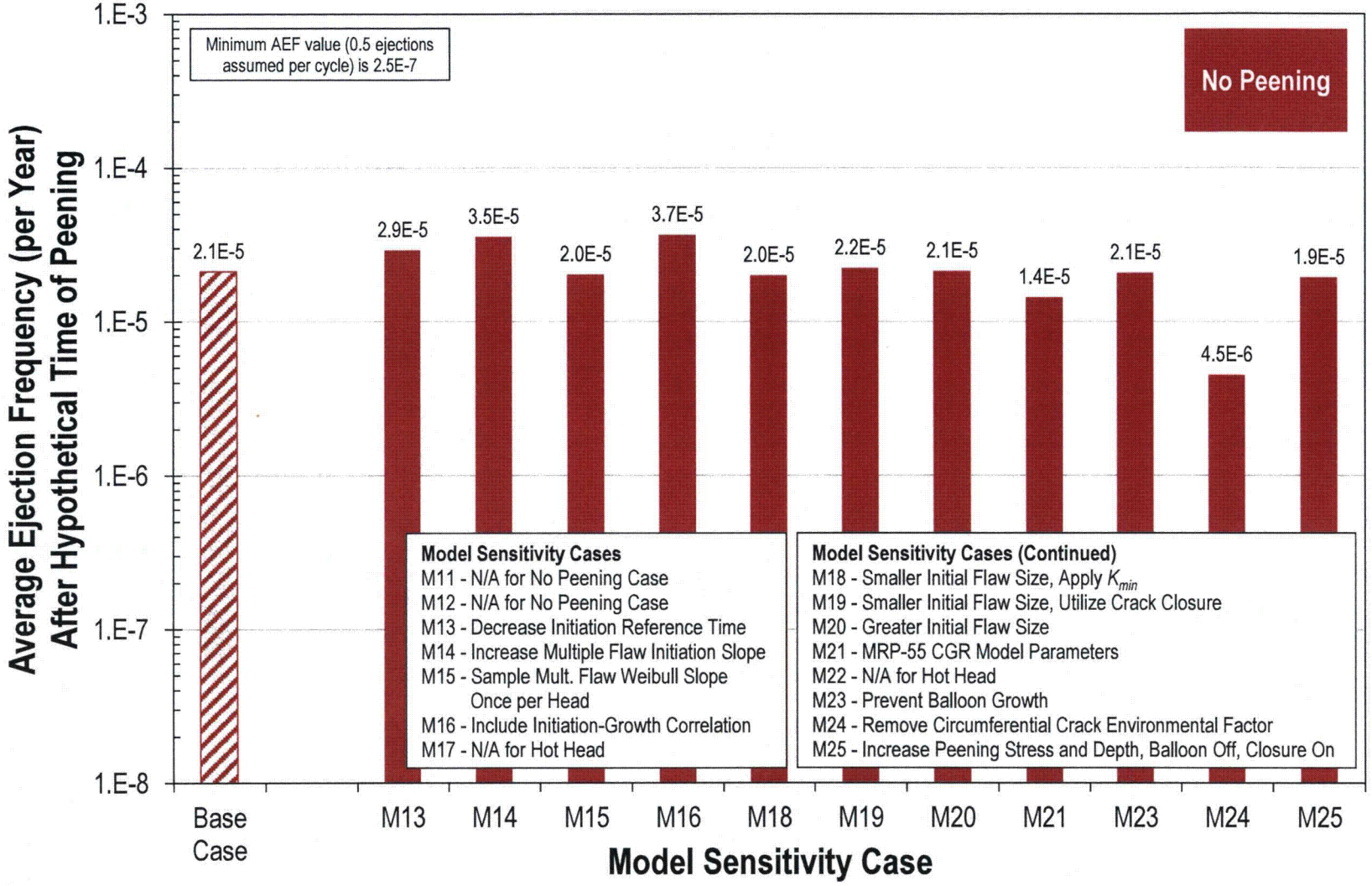

Figure B-15
Summary of Model Sensitivity Results for Hot RPVHPN Probabilistic Model without Peening (Continued)

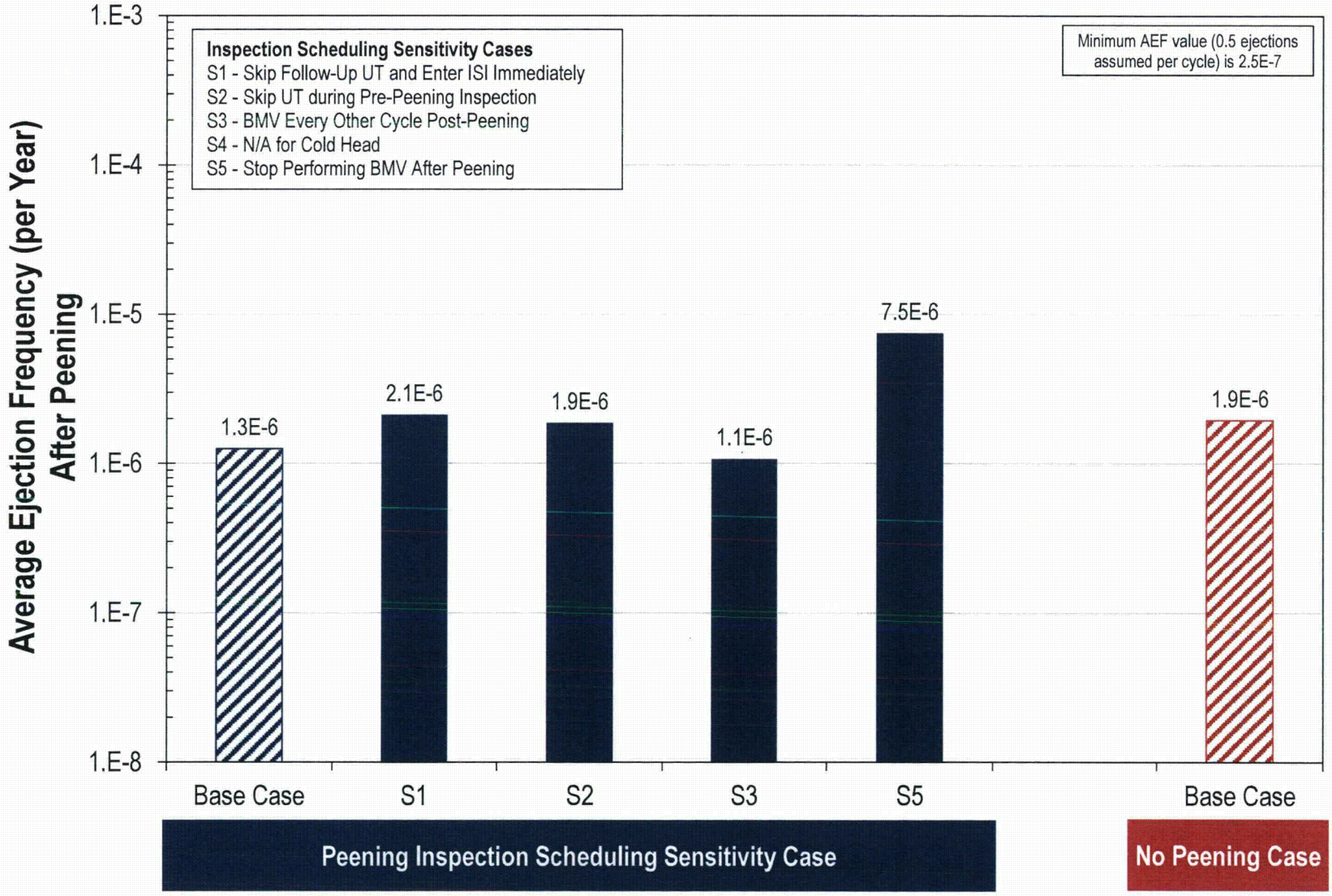

Figure B-16
Summary for Inspection Scheduling Sensitivity Results for Cold RPVHPN Probabilistic Model with Peening

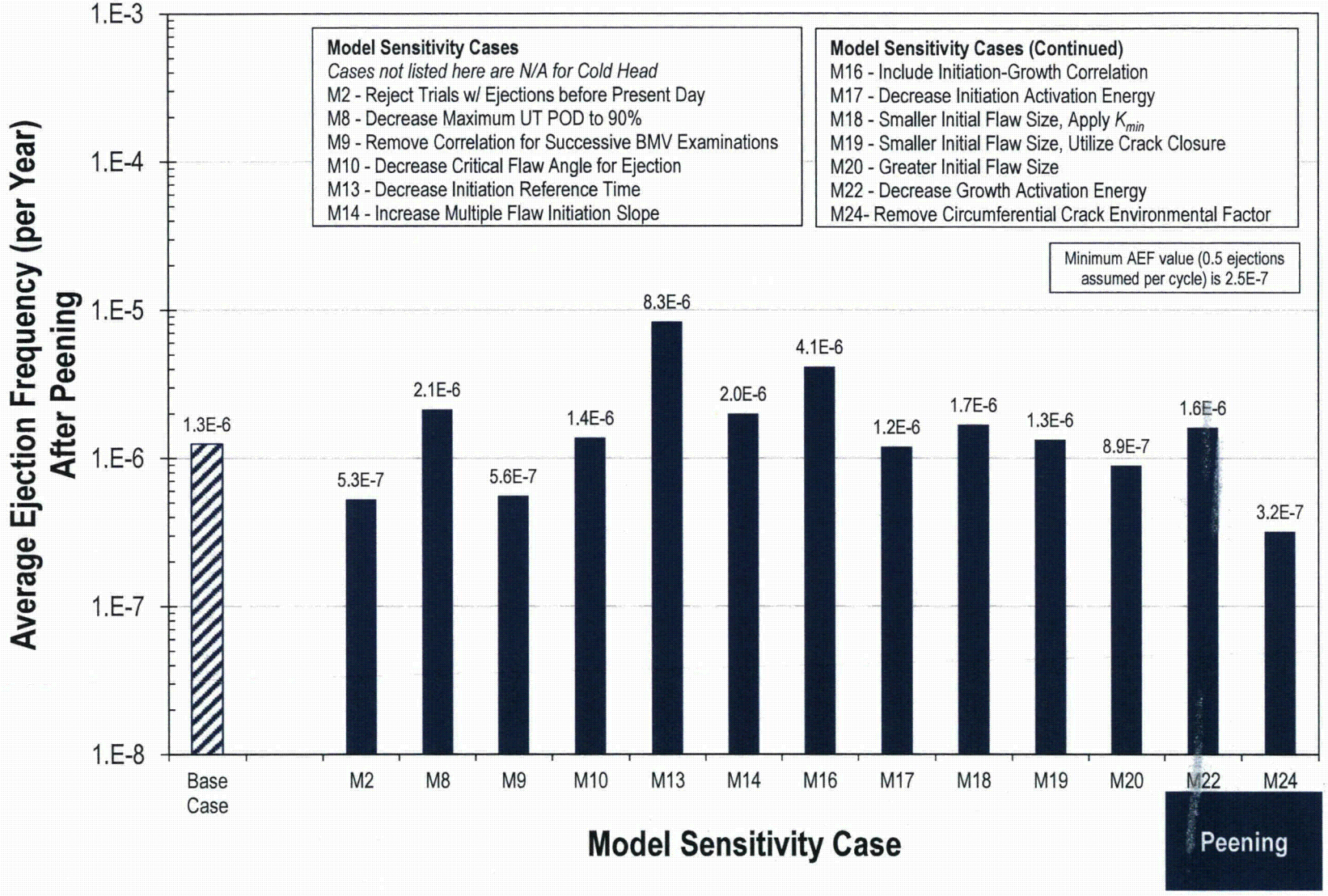

Figure B-17
Summary of Model Sensitivity Results for Cold RPVHPN Probabilistic Model with Peening

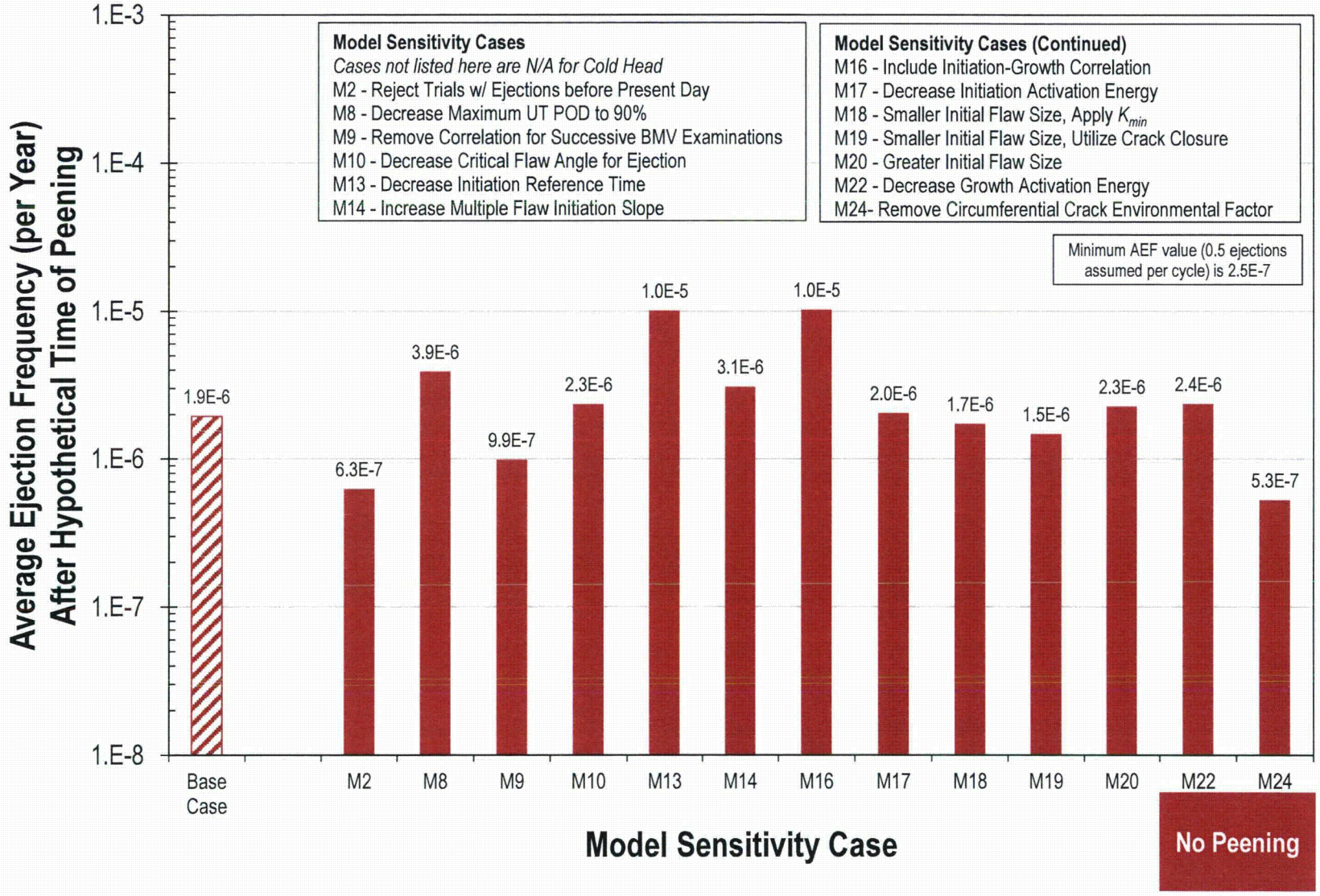

Figure B-18
Summary of Model Sensitivity Results for Cold RPVHPN Probabilistic Model without Peening

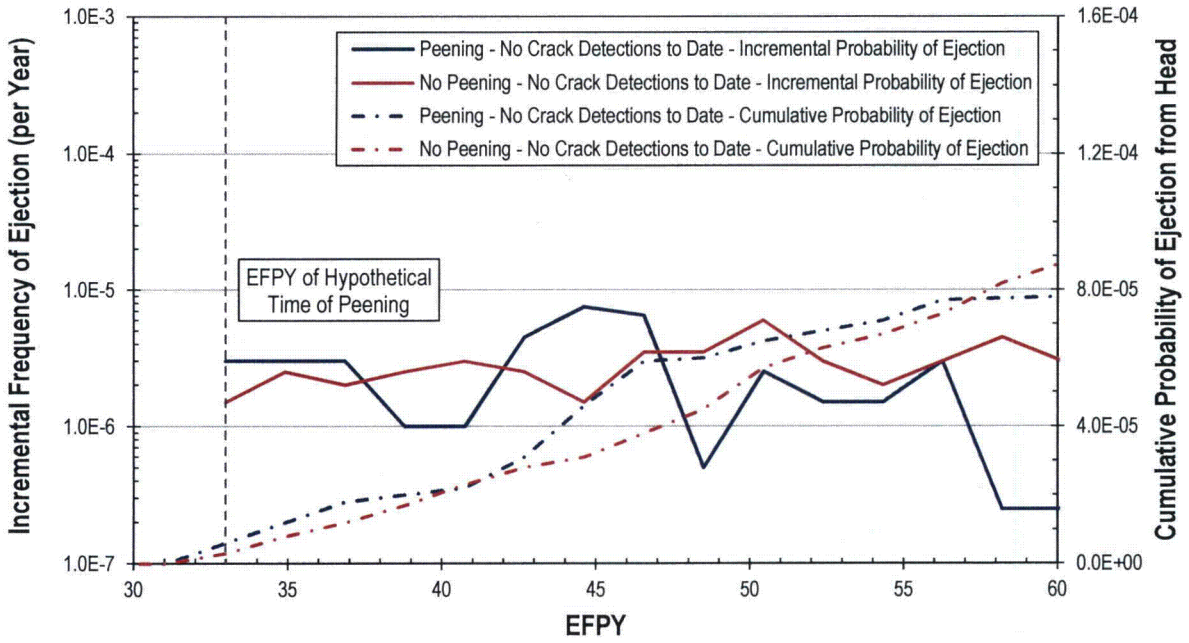

Figure B-19
Prediction of Nozzle Ejection vs. Time for Hot RPVHPNs with No Crack Detections to Date (Model Sensitivity Study 2)

B.4 References

1. *Materials Reliability Program: Topical Report for Primary Water Stress Corrosion Cracking Mitigation by Surface Stress Improvement (MRP-335, Revision 1).* EPRI, Palo Alto, CA: 2013. 3002000073. [Freely Available at www.epri.com]
2. U.S. NRC, Second Request for Additional Information for MRP-335, Revision 1, "Topical Report for Primary Water Stress Corrosion Cracking Mitigation by Surface Stress Improvement (Peening)" (TAC No. MF2429), April 2, 2015. [NRC ADAMS Accession No.: ML15057A028]
3. *Materials Reliability Program: Reevaluation of Technical Basis for Inspection of Alloy 600 PWR Reactor Vessel Top Head Nozzles (MRP-395).* EPRI, Palo Alto, CA: 2014. 3002003099. [Freely Available at www.epri.com]
4. ASME Code Case N-729-1, "Alternative Examination Requirements for PWR Reactor Vessel Upper Heads With Nozzles Having Pressure-Retaining Partial-Penetration Welds," Section XI, Division 1, American Society of Mechanical Engineers, New York, Approval Date: March 28, 2006.
5. *xLPR Pilot Study Report*. U.S. NRC-RES, Washington, DC, and EPRI, Palo Alto, CA: NUREG-2110 and EPRI 1022860. 2012. [Freely Available at www.epri.com]
6. Materials Reliability Program (MRP) Crack Growth Rates for Evaluating Primary Water Stress Corrosion Cracking (PWSCC) of Thick-Wall Alloy 600 Materials (MRP-55) Revision 1, EPRI, Palo Alto, CA: 2002. 1006695. [Freely Available at www.epri.com]
7. *Materials Reliability Program Crack Growth Rates for Evaluating Primary Water Stress Corrosion Cracking (PWSCC) of Alloy 82, 182, and 132 Welds (MRP-115)*, EPRI, Palo Alto, CA: 2004. 1006696. [Freely Available at www.epri.com]
8. *Materials Reliability Program: Probabilistic Fracture Mechanics Analysis of PWR Reactor Pressure Vessel Top Head Nozzle Cracking (MRP-105 NP)*, EPRI, Palo Alto, CA: 2004. 1007834. [NRC ADAMS Accession No.: ML041680489]
9. *Materials Reliability Program: Reactor Vessel Closure Head Penetration Safety Assessment for U.S. PWR Plants (MRP-110NP): Evaluations Supporting the MRP Inspection Plan*, EPRI, Palo Alto, CA: 2004. 1009807-NP. [NRC ADAMS Accession No.: ML041680506]
10. U.S. NRC, Regulatory Guide 1.174, "An Approach for Using Probabilistic Risk Assessment in Risk-Informed Decisions on Plant-Specific Changes to the Licensing Basis," Revision 2, May 2011. [NRC ADAMS Accession No. ML100910006]

C
TENSILE BALANCING STRESSES IN RESIDUAL STRESS PROFILE IN RESPONSE TO PEENING

C.1 Introduction

C.1.1 Deformation and Tensile Stress Response of Components to Peening

In addition to producing a surface compressive residual stress layer, peening causes deformation of the treated component. Some of the compressive stress at the peened layer is immediately relieved by deformation of the part. As the stiffness of the treated component is assumed to be greater, the resulting deformation decreases, and more of the initial compressive stress at the treated surface is retained.

The retained compressive stress at the peened surface is balanced by residual stresses generated through the component thickness. In order to satisfy static equilibrium, the internal forces and internal bending moments integrated over any cross section through the component must balance to zero or be balanced by a reaction force on the component. If the through-wall stress profile is suitably uniform over a cross section (and the plate length-to-width aspect ratio is suitable large such that beam theory holds), the residual stress profile for an unrestrained flat plate must self-balance by force and through-wall bending moment before and after peening. Thus, the peak balancing tensile stress in the post-peening through-wall profile for an unrestrained flat plate depends on both the force and moment imparted by the surface compressive stress layer.

The balancing stress for peened thick-wall pipes behaves in a similar manner, but the more constrained pipe geometry does not deflect as much as the plate case for equivalent peening compressive stress effect and equivalent wall thickness. As shown in the analyses presented below, the result is that the balancing stress profile for a thick-wall pipe is more nearly uniform than for the case of an unrestrained flat plate of equivalent wall thickness.

C.1.2 Purpose and Approach

The purpose of this attachment is to investigate the magnitude and distribution of tensile stresses developed in response to the peening compressive stresses produced at the treated surface. Any pre-existing flaws located beyond the compressive stress zone would grow during subsequent operation under the influence of these balancing stresses (as well as weld residual stresses and operating stresses).

Specifically, a straightforward linear-elastic finite-element analysis (FEA) approach is taken for flat plate and thick-wall cylinder geometries. Peening is assumed to be applied to a substantial fraction of the plate area or inside diameter surface of a thick-walled cylinder, and the through-wall stress profile developed in the peened region is investigated for different wall thicknesses. The stress source approach ([1], [2], [3]) originally developed to assess the stress effects of shot

peening of a flat plate is applied to calculate the bending stress and axial membrane stress generated in response to peening:

$$\sigma(x) = \sigma_p(x) + \sigma_b(x) + \sigma_a \qquad [C\text{-}1]$$

where:

$\sigma(x)$ = through-wall equilibrium stress profile, as function of through-wall position x

$\sigma_p(x)$ = peening stress source function

$\sigma_b(x)$ = bending stress generated in response to peening (linear function of x)

σ_a = axial membrane stress generated in response to peening

The stress source function, $\sigma_p(x)$, is the stress that would result from peening of an infinitely thick plate. For sufficiently thick plates, the stress source depends only on the peening process applied (i.e., intensity and duration). The form of the stress source function is chosen to fit data for the particular peening process of interest. As described below, published data are used to determine the most appropriate form of the stress source function. Published stress measurements and modeling results also illustrate the expected trends.

The stress source function is imposed in the FEA model as an initial condition for the stress state in the region of the "peened" surface, and the FEA solver is used to calculate the equilibrium stress response. The two-dimensional FEA model for the unrestrained flat plate case is used to demonstrate how more of the compressive stress near the surface is retained as the wall thickness is increased for a constant peening intensity (i.e., stress source function). Additional cases for the flat plate geometry show how the equilibrium stress profile, including the peak tensile stress, varies with wall thickness while holding constant the amount of compressive stress retained at the "peened" surface (surface magnitude and compressive depth) by varying the stress source function. These results are then extended to the thick-wall cylinder geometry.

The form of the stress source function is validated based on a published set of experimental stress measurements performed on a peened flat plate. The FEA approach is further validated through application of a simple bilinear stress profile that is analytically constrained to satisfy through-wall force and moment balances.

The FEA model is described in Section C.2, the simulated cases are listed in Section C.3, the results are presented in Section C.4, and the model validation is presented in Section C.5. Conclusions are made in Section C.6.

C.1.3 Relevant Literature

Researchers have studied tensile balancing effects in post-peening residual stress profiles in a range of geometries for shot peening, laser peening, and water-jet peening. The following findings are relevant to the tensile balancing stress in the post-peening residual stress profile:

- Buchannan and John [4] show that for a constant residual surface stress, the peak tensile stress decreases as component thickness increases. With increased component thickness, the

balancing force is spread over a greater distance and the difference in balancing tensile stress required to develop a balancing through-wall moment is decreased.

- Hill, et al. [5] show that the peak tensile stress indirectly induced by a peening process decreases as the compressive residual stress at the surface decreases. As the peening intensity is increased and a larger compressive surface stress is produced, the peak tensile stress beyond the compressive layer tends to increase.
- Menig, et al. [6] investigated the nature of the tensile stress field beyond the peening compressive layer. The results presented in this paper indicate that the compressive residual stresses generated by peening are balanced by rather low tensile residual stresses extending over the whole cross-section of the component.
- DeWald and Hill [7] measured stresses and performed strain and stress modeling for four different specimen geometries treated by laser peening, including thick-wall cylinders peened on the outer diameter. The through-wall residual stress measurements were made using the contour method. The stress profile measured for the thick-wall cylinder case is comparable to that observed in other studies for peening of flat plates, although the profile near the inside surface (not peened) showed greater curvature than for flat plate cases. This case is not directly applicable to peening of reactor vessel primary nozzles because the peening was performed on the OD and because of the especially small inner-radius-to-thickness ratio, $R_i / t = 15$ mm / 15 mm = 1.0.

C.2 ANSYS Model Description

A two-dimensional linear-elastic ANSYS [8] FEA model is used to simulate the balancing stress effects of either:

(1) a cross section of a flat plate peened on one side, or

(2) a thick-wall pipe that is subjected to axisymmetric peening on the pipe inside surface.

The peening process itself is not simulated. Instead the balancing stress profile generated in response to the peening compressive stress layer at the treated surface is calculated considering the effect of the component geometry and stiffness. The standard peening stress source approach, also known as the "eigenstress" approach, is taken in which the initial stress profile due to peening (prior to deformation of the component and development of the balancing stress) is directly input to the model as an initial condition. This initial stress source function is independent of the component geometry given a sufficiently large wall thickness. The final stress state at equilibrium, which reflects both the reduction in peening compressive stress due to component deformation as well as generation of the balancing residual stress, is calculated using the ANSYS FEA solver. Although the peening process itself results in substantial local yielding and plastic strains, the redistribution of stress beyond the surface compressive residual stress zone in response to peening is an elastic unloading problem [1], and thus amenable to the linear-elastic stress source approach.

The material properties, geometry, boundary conditions, and loading are described in the following subsections.

C.2.1 Material Properties

The ANSYS model is a linear-elastic model. Thus the needed properties are limited to Young's Modulus and Poisson's Ratio. As shown in Table C-1, room-temperature values were input using the physical properties tabulated in Section II Part D of the ASME Boiler and Pressure Vessel Code [9] for Alloy 600 and another nickel-based alloy, Alloy 22. The material properties for Alloy 22 were applied in the case used to validate the chosen form of the stress source function.

Table C-1
Material Properties [9]

Material	Parameter	Units	Value
Alloy 600	Young's Modulus	Pa	2.13E+11
	Poisson's Ratio	-	0.31
Alloy 22	Young's Modulus	Pa	2.06E+11
	Poisson's Ratio	-	0.31

C.2.2 Geometry

The same two-dimensional mesh is used to model a flat plate or an axisymmetric pipe. The ANSYS PLANE183 element type is applied under the generalized plane strain assumption for the flat plate geometry and in axisymmetric mode for the pipe geometry.

It was shown that the choice of either generalized plane strain or plane stress for the plate geometry does not significantly affect the in-plane stress results presented in this attachment. The reason is that the calculated profile for the in-plane (Y-direction) stress must satisfy the same force and moment balances regardless of whether the plane strain or plane stress assumption is made for two-dimensional treatment of Hooke's Law.

The geometry of the plate and pipe models is defined by the example mesh shown in Figure C-1. When modeling a plate, the model can be considered to be infinitely wide in the out-of-plane direction. When modeling a pipe, the out-of-plane direction is the azimuthal dimension and the axis of rotation is to the left of the mesh of Figure C-1. The pipe geometry boundary conditions make the pipe behave as though it is infinite in length. As shown in red in this figure, the model includes a distinct area on the left (inner diameter) surface where the stress source function is applied to simulate the effects of peening. This area is assigned an initial stress profile, as described by Section C.2.4, to model the effects of peening while the initial stress state in the remainder of the mesh is zero.

The mesh spacing is controlled in the model to ensure the results are accurate in the areas of interest. The mesh is refined in the region where the stress source function is applied because this is the area with the largest stress gradient. The effect of overall mesh refinement was checked to confirm model convergence. The length of the peened area is chosen to result in a region of reasonably uniform stresses that are reasonably fully developed without edge effects, and the solution is confirmed to be converged with respect to the modeled length of the mesh. The modeled geometry satisfied a study of the spatial uniformity of the peak stress and of the compressive stress layer depth.

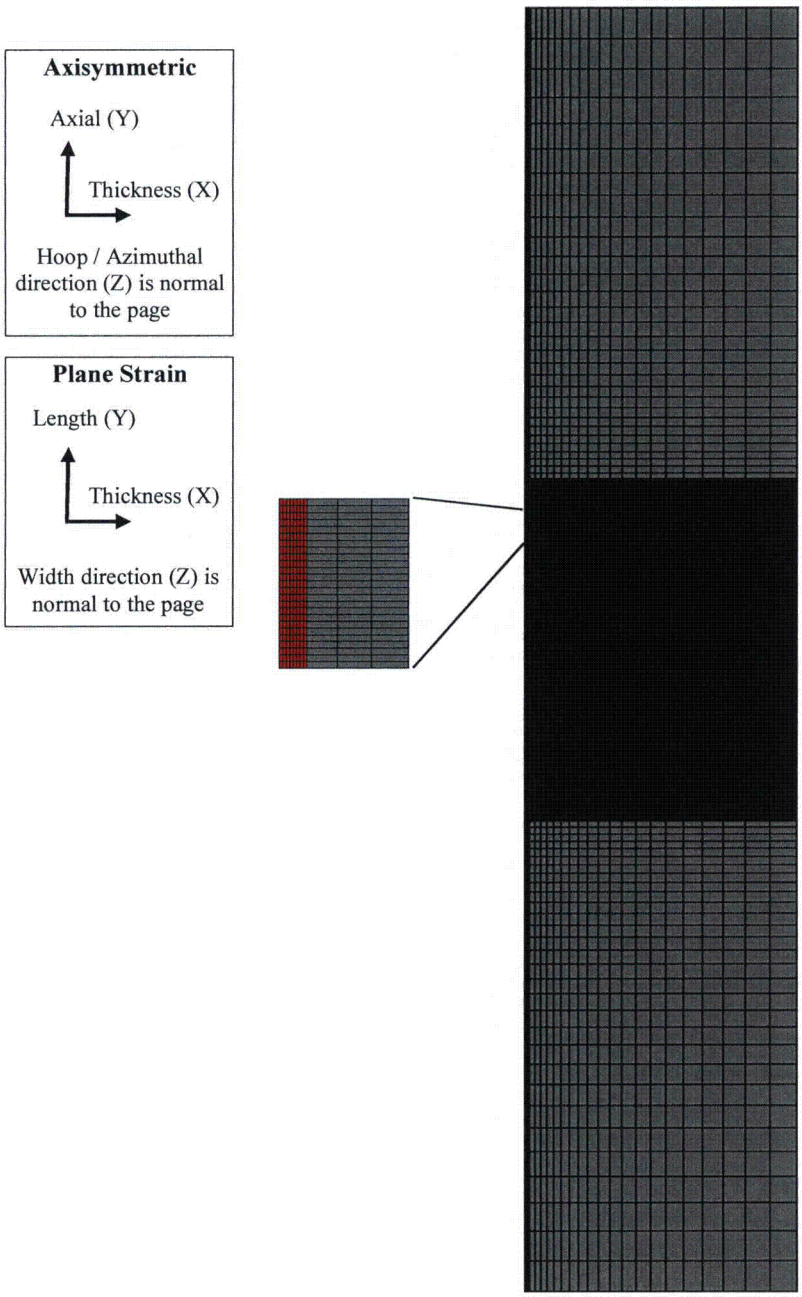

Figure C-1
Example Mesh with Region of Application of Stress Source Function in Red (wall thickness = 63.5 mm)

C.2.3 Boundary Conditions

To prevent rigid-body motion of the model, the following boundary conditions are applied:

Flat Plate Geometry

- Midpoint of Left Side of Cross Section: Zero displacement in the X- and Y-directions
- Midpoint of Right Side of Cross Section: Zero displacement in the Y-direction

Thick-Wall Pipe Geometry

- Bottom Row of Nodes: Zero displacement in Y-direction
- Top Row of Nodes: Displacement in Y-direction is uniformly the same (coupled)

C.2.4 Loading

The only load source in the model is the biaxial initial stress state specified in the region where the stress source function is applied. The initial stress state is specified using the ANSYS INISTATE command and applied to the nodes of the elements in the stress source region according to the nodal position. The profile is applied to both the SY and SZ stress components. No initial stress is input for the through-thickness component (SX).

Per the validation exercise described below in Section C.4.1, the stress source function is assumed to have an exponential form. An improved fit to the validation data resulted from a small refinement to a pure exponential decay function. The stress source function is based on an exponential function scaled to reach zero at a depth of δ_p:

$$\sigma_p(x) = \sigma_{p,0}\left[\frac{e^{-x/\tau} - R}{1 - R}\right] \quad \text{for } x < \delta_p$$

$$\tau = -\frac{\delta_p}{\ln(R)} \qquad \text{[C-2]}$$

where:

δ_p	=	depth of region subjected to initial stress source function
x	=	through-wall depth from "peened" surface
$\sigma_p(x)$	=	peening stress source function
$\sigma_{p,0}$	=	initial peening compressive stress at peened surface prior to deformation
R	=	fraction of exponential remaining at $x = \delta_p$, taken to be 0.04 based on the comparison in Section C.4.1

Examples of a stress source function having the form of Equation [C-2] and the final equilibrium stress state in the component are shown in Figure C-2 and Figure C-3.

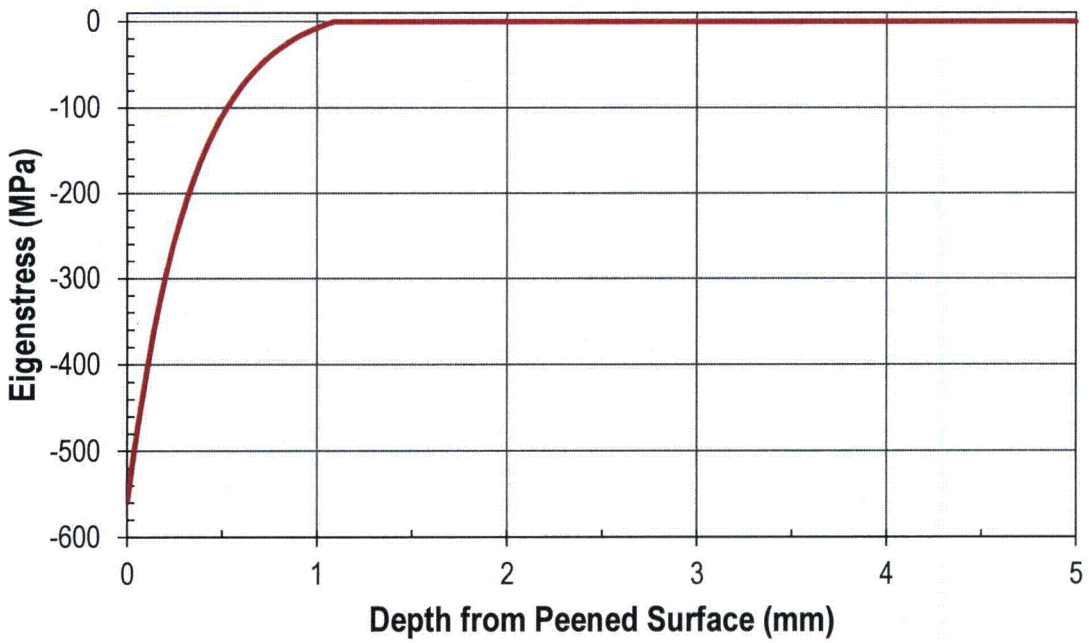

Figure C-2
Example Stress Source Function for $\sigma_{p,0}$ = -558 MPa (-80.9 ksi) and δ_p = 1.09 mm (0.043 in.)

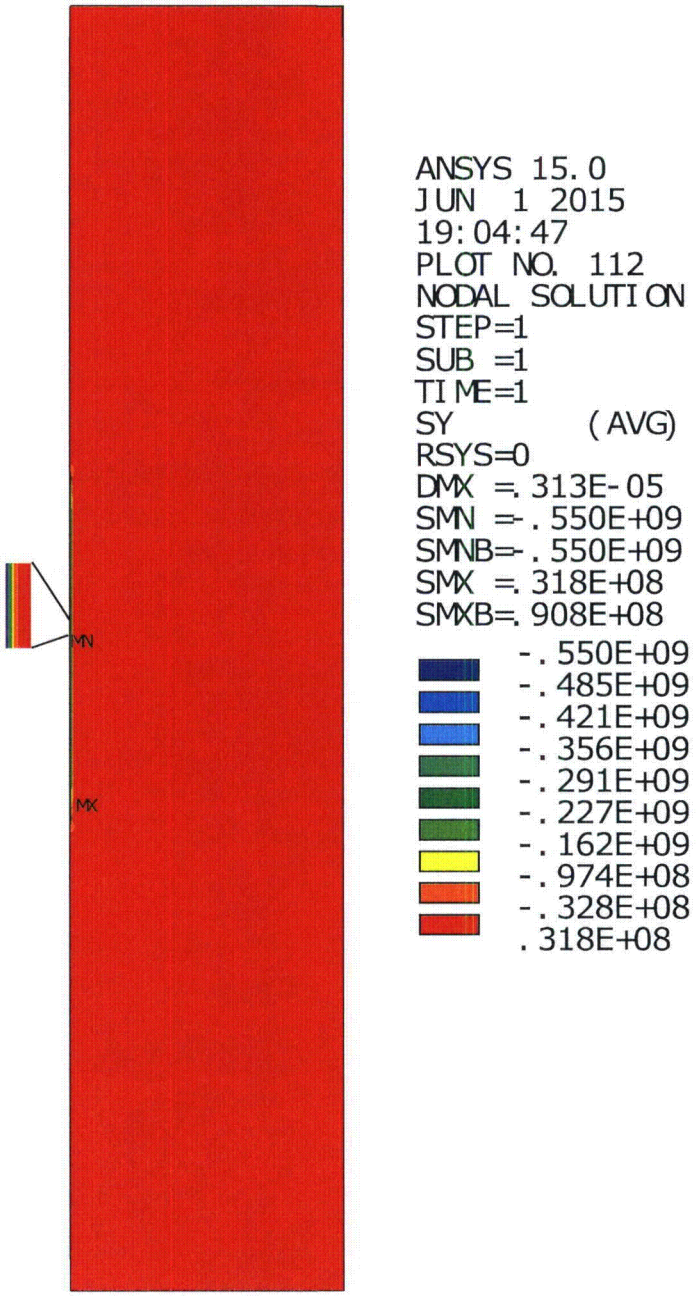

Figure C-3
Example Equilibrium Stress Solution Contour Plot for the Length (Y) Direction Stress (SY) for Flat Plate Model (wall thickness = 63.5 mm)

C.3 ANSYS Model Cases

The FEA model was used to investigate the following cases:

- **Validation of Exponential Form of Stress Source Function**
  - Simulates the stress profile for a flat plate treated by laser peening (measured by Hill et al. [5]) (Figure C-4)
  - Material: Alloy 22
  - Plate with thickness of 20 mm and length of 38 mm
  - Peened area length of 30 mm
  - Modeled using an equilibrium surface compressive stress of ~470 MPa (68.2 ksi) and depth of 2.74 mm
- **Plate with Thickness of Reactor Vessel Outlet Nozzle (Two-Dimensional)**
  - Simulates an unrestrained flat plate with thickness comparable to the reactor vessel outlet nozzle pipe case to show the effect of modeling a plate vs. a pipe. The simpler plate geometry is a common geometry for published testing and modeling efforts.
  - Material: Alloy 600
  - Plate length of 300 mm and peened area length of 80 mm
  - Plate wall thickness:
    - Base case thickness of 2.5 inches (63.5 mm), which is close to the lower bound thickness of 2.4 inches (61 mm) cited in MRP-109 [10]
    - Sensitivity cases illustrating effect of wall thickness ranging from a factor of 8 thinner to a factor of 6 thicker
  - Peening stress source function assumptions:
    - Constant stress source function ($\sigma_{p,0}$ = -558 MPa (-80.9 ksi) and δ_p = 1.09 mm) to illustrate greater retention of initial compressive stress as thickness is increased
    - Vary stress source function to obtain equilibrium surface compressive stress of ~550 MPa (80 ksi) and compressive stress depth of 1.0 mm
- **Reactor Vessel Outlet Nozzle (Axisymmetric)**
  - Simulates effects of peening on the ID of a thick-wall pipe with the dimensions of a typical reactor vessel outlet nozzle (RVON) dissimilar metal weld.
  - Material: Alloy 600
  - Pipe length of 300 mm, peened area length of 80 mm, and ratio of inner radius to thickness of 5.8 (yields an outer diameter of 34 inches (864 mm) for a thickness of 2.5 inches (63.5 mm))
  - Pipe wall thickness:
    - Base case thickness of 2.5 inches (63.5 mm), which is close to the lower bound thickness of 2.4 inches (61 mm) cited in MRP-109 [10]
    - Sensitivity cases illustrating effect of wall thickness ranging from a factor of 8 thinner to a factor of 6 thicker (evaluated both for a constant outer diameter of 34 inches and for a constant ratio of inner radius to wall thickness of 5.8)

- Peening stress source function assumptions:
  - Vary stress source function to obtain equilibrium surface compressive stress of ~550 MPa (80 ksi) and compressive stress depth of 1.0 mm
  - Sensitivity cases illustrating effect of compressive stress depth using 0.5 mm and 1.5 mm equilibrium surface compressive stress depths for RVON base case dimensions

C.4 ANSYS Model Results

C.4.1 Validation of Exponential Form of Stress Source Function

The parameters for the exponential stress source function ($\sigma_{p,0}$ and δ_p in Equation [C-2]) were varied until the match between the measured stress profile and the calculated equilibrium profile in Figure C-4 was obtained. The magnitude of the peak stress obtained in this case reflects the magnitude of the compressive stress depth (2.7 mm) in comparison to the wall thickness (20 mm).

The very good agreement between the measured and predicted stress profiles shows that the exponential form of Equation [C-2] is a good choice to model the peening effect for the type of laser peening performed by Hill et al. [5]. Furthermore, the measured peening compressive stress profiles presented in MRP-267 Rev. 1 [11] for a variety of laser peening and water jet peening processes have shapes that are generally reasonably approximated by the shape of the peening compressive stress profile measured by Hill et al. [5] and shown in Figure C-4. Hence, the stress source functional form defined in Equation [C-2] is applied in all the FEA cases.

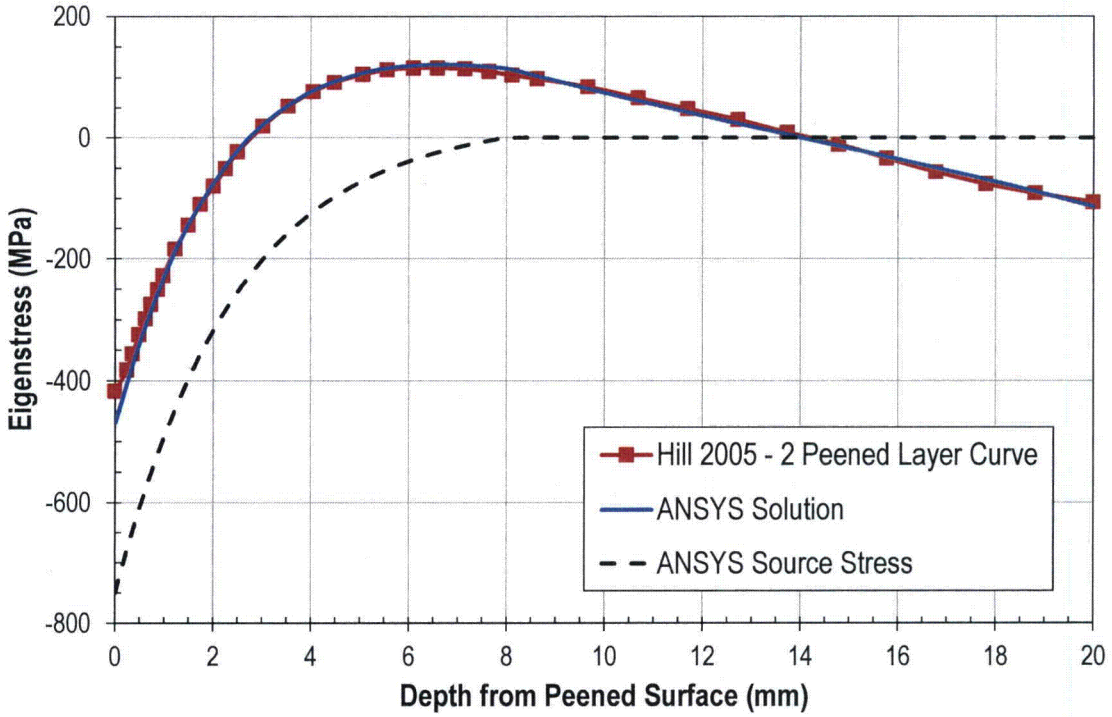

Figure C-4
Validation of Exponential Form of Stress Source Function Using Through-Wall Stress Profile Measured by Hill et al. [5]

C.4.2 Calculated Stress Profiles for Flat Plate and Thick-Wall Pipe Geometries

The FEA analyses results are shown in Figure C-5 through Figure C-13, where in each figure the stress profile is taken at the midpoint of the peened region (i.e., the symmetry plane of the model):

Effect of Wall Thickness on Retained Peening Compressive Stress (Flat Plate)

- Figure C-5 illustrates how the compressive stress effect developed by peening increases (in terms of surface compressive stress magnitude and compressive stress depth) for the same peening intensity as the wall thickness is increased. More of the initial peening compressive stress would be retained for the thick-wall pipe geometry for equivalent wall thickness because of its greater level of constraint. Because the peening performance criteria are based on the stress profile achieved following peening (including the relaxation in compressive stress at the surface due to elastic deformation of the component upon peening), the results presented below for a consistent equilibrium compressive stress effect are more important to the conclusions of this investigation.

Effect of Wall Thickness on Balancing Stress Profile (Flat Plate and Thick-Wall Pipe)

- Figure C-6 clearly illustrates how the peak tensile stress is reduced as the wall thickness is increased for the flat plate geometry with the stress source function parameters varied to obtain constant equilibrium values of the surface compressive stress magnitude and compressive depth. The profiles show how a linear stress profile (through-wall bending) and an axial membrane stress component are produced in response to the peening effect. As discussed by Bernasconi and Roth [1], this is the expected behavior of a peened plate and reflects simple beam behavior. Note that it was numerically confirmed that these calculated stress profiles satisfy both force and moment balance. This is a requirement of the model since the through-thickness profile for stress in the Y-direction is necessarily uniform in the Z-direction (into the page) given the two-dimensional assumption.
- Figure C-7 shows similar behavior for the axial stress profile for the thick-wall pipe geometry. For equivalent wall thickness, the peak tensile stress is smaller for the pipe axial stress case. The pipe geometry is more constrained than a flat plate and does not deflect as much as the plate case for equivalent peening compressive stress effect and equivalent wall thickness. The reduced curvature for the pipe case means that a smaller through-wall bending stress component is produced in the axial direction than would be the case for the corresponding flat plate. In addition, the gradient in cross sectional area between the inner and outer portions of the pipe cross section tends to increase the contribution of a given through-wall stress gradient to the through-wall force and bending moment in comparison to the situation for a flat plate. Note that it was numerically confirmed that these calculated stress profiles satisfy force balances. Force balance over a given through-wall profile is a requirement of the model since the axial stress profile is necessarily uniform in the azimuthal direction given the axisymmetric assumption. The pipe geometry does not satisfy the moment balance in the same manner as for the unrestrained flat plate as shear stresses contribute to the balance for the pipe.
- While the results in Figure C-7 represent a constant outer diameter while the thickness is varied, Figure C-8 plots the equivalent axial stress results for a constant inner-radius-to-thickness ratio. The peak tensile stress for the pipe geometry cases remains smaller than the peak tensile stress in the plate geometry case for equivalent wall thickness. Note that the curves with a positive slope in Figure C-8 have a lower peak tensile stress than the equivalent constant outer diameter curves (having a negative slope). These cases with positive slope correspond to relatively small wall thicknesses and are the result of a more complex deformed shape of the pipe compared to cases with greater wall thickness or greater diameter. It was numerically confirmed that these calculated stress profiles also satisfy force balance.
- Figure C-9 and Figure C-10 show the calculated profiles for the case of the hoop stress for the thick-wall pipe geometry. Note that the compressive stress depth at equilibrium for the hoop stress profile varies slightly for the different thickness cases because the stress source function was varied to maintain the compressive stress depth for the axial stress profile. Regardless of this point, the magnitude of the tensile stress response is substantially smaller for the hoop stress profile in comparison to that for the axial stress for equivalent wall thickness. This lower peak magnitude occurs because the force balance in the hoop direction is enforced over the entire modeled area, permitting a

distribution of the tensile balancing stress over a greater area. The hoop profiles have smaller slopes than the axial profiles because the axial change in curvature upon peening is greater than the change in curvature of the pipe in the circumferential direction. The pipe geometry is most constrained in the circumferential direction.

Effect of Wall Thickness on Peak Balancing Tensile Stress (Flat Plate and Thick-Wall Pipe)

- Figure C-11 and Figure C-12 plot the peak tensile stress of the profiles in Figure C-6 through Figure C-10 directly as a function of wall thickness. The peak tensile stress is plotted as a percentage of the surface compressive stress value as the shape of the stress profile does not depend on the magnitude of the surface compressive stress.

Effect of Peening Compressive Stress Depth on Balancing Stress Profile (RVON Pipe Geometry)

- The results in Figure C-6 through Figure C-12 assumed a post-peening compressive stress depth of 1 millimeter. Figure C-13 illustrates how the axial stress profile for the RVON geometry is affected by this assumption. Profiles are shown for compressive depths of 0.5 mm and 1.5 mm in addition to 1.0 mm. The magnitude of the peak tensile stress has an approximate linear dependence on the compressive stress depth. This is expected given that the force and moment created by the compressive profile close to the peened surface are each approximately proportional to the compressive depth.

As shown in the figures, the calculated maximum tensile stress for a given peening compressive stress effect (surface magnitude and compressive depth) decreases with increasing wall thickness. This applies in both the axial and hoop directions for the pipe.

For the reactor vessel outlet nozzle (RVON) thick-wall pipe geometry, the peak tensile balancing stresses are less than about 2% of the magnitude of the compressive surface stress for the case of a compressive stress layer at the pipe ID that is 1 millimeter deep. This relatively small magnitude for the peak tensile balancing stress is the result of the balancing force and moment being spread over the large wall thickness of this component, plus the fact that the pipe geometry is more constrained than a flat plate and does not deflect as much as the plate case for equivalent peening compressive stress effect and equivalent wall thickness.

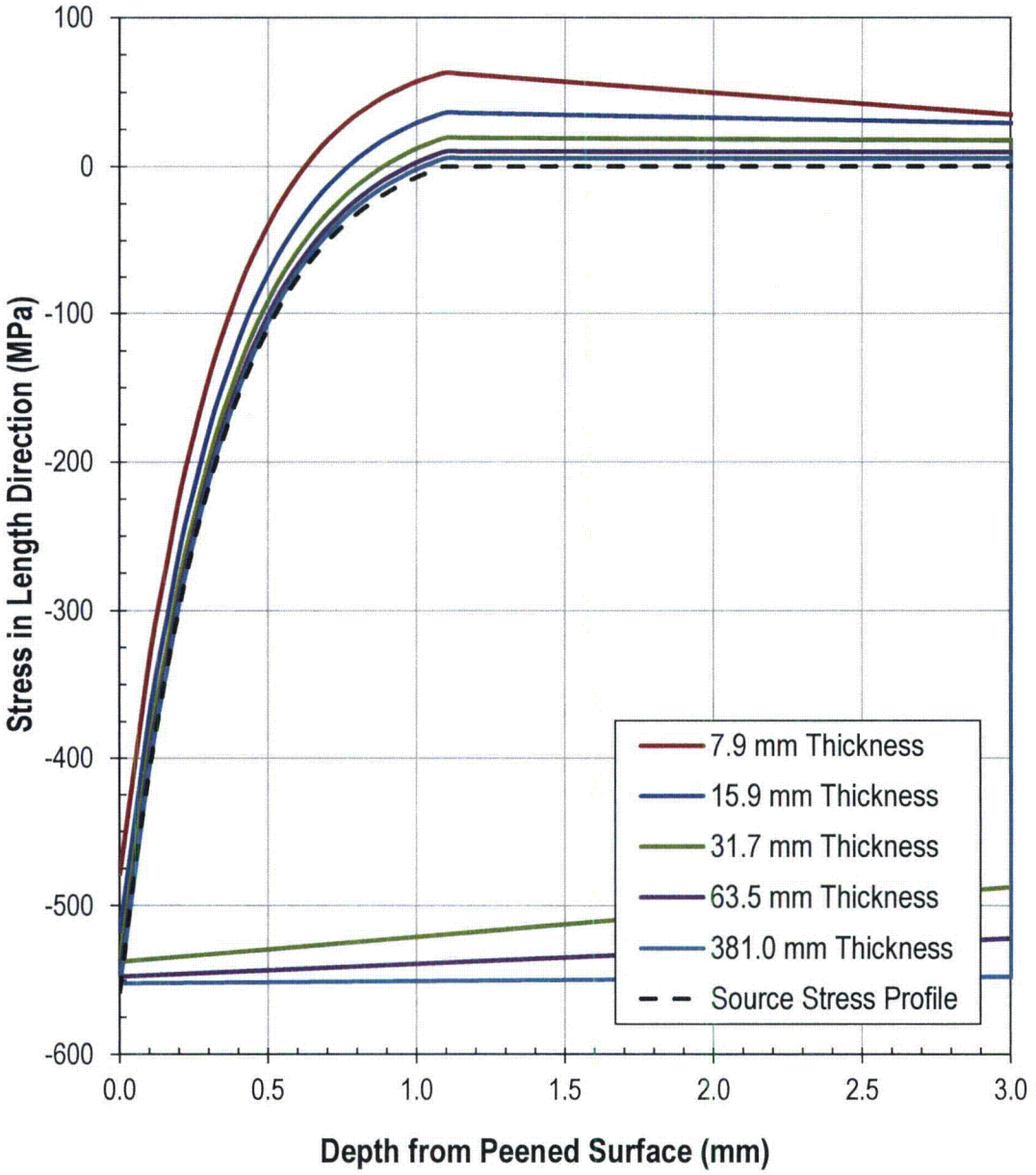

Figure C-5
Equilibrium Through-Wall Stress Profiles for Flat Plate for Common Stress Source Function

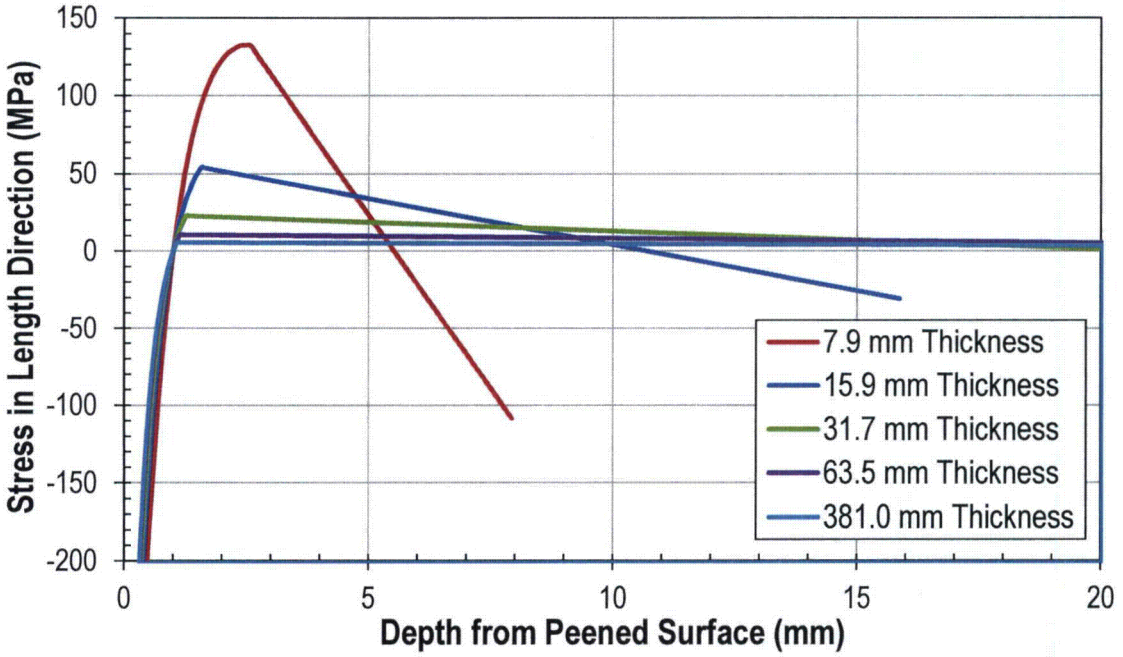

Figure C-6
Effect of Wall Thickness on Through-Wall Stress Profile for Plate Geometry for Same Equilibrium Surface Compressive Stress and Compressive Depth

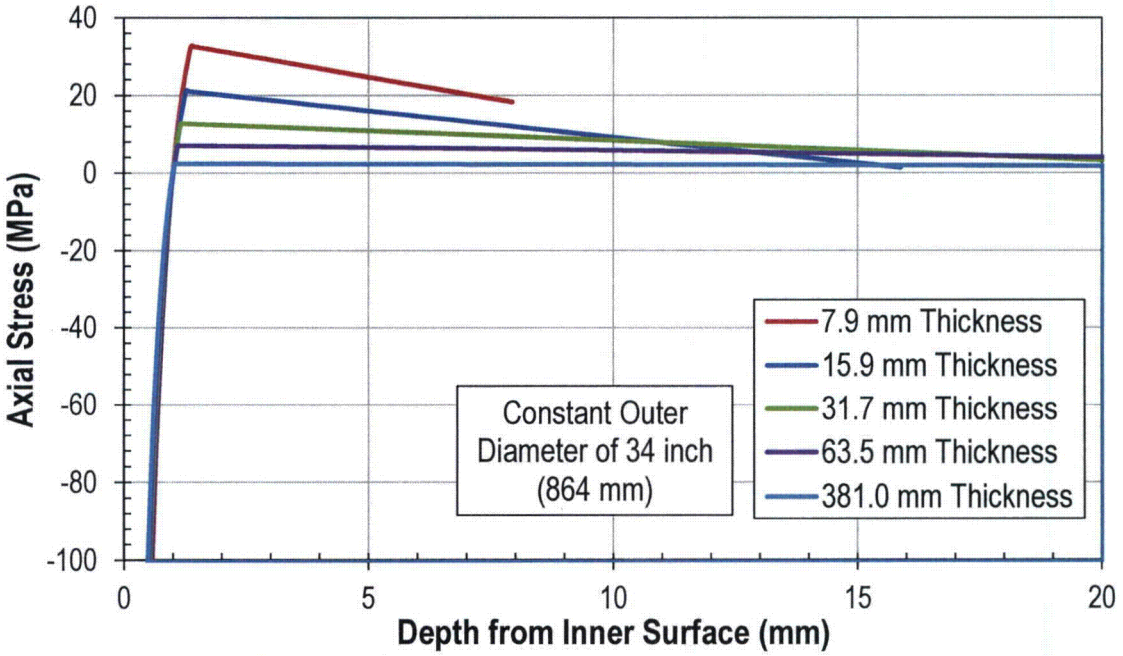

Figure C-7
Effect of Wall Thickness on Through-Wall Axial Stress Profile for Constant Outer Diameter Pipe Geometry for Same Equilibrium Surface Compressive Stress and Compressive Depth

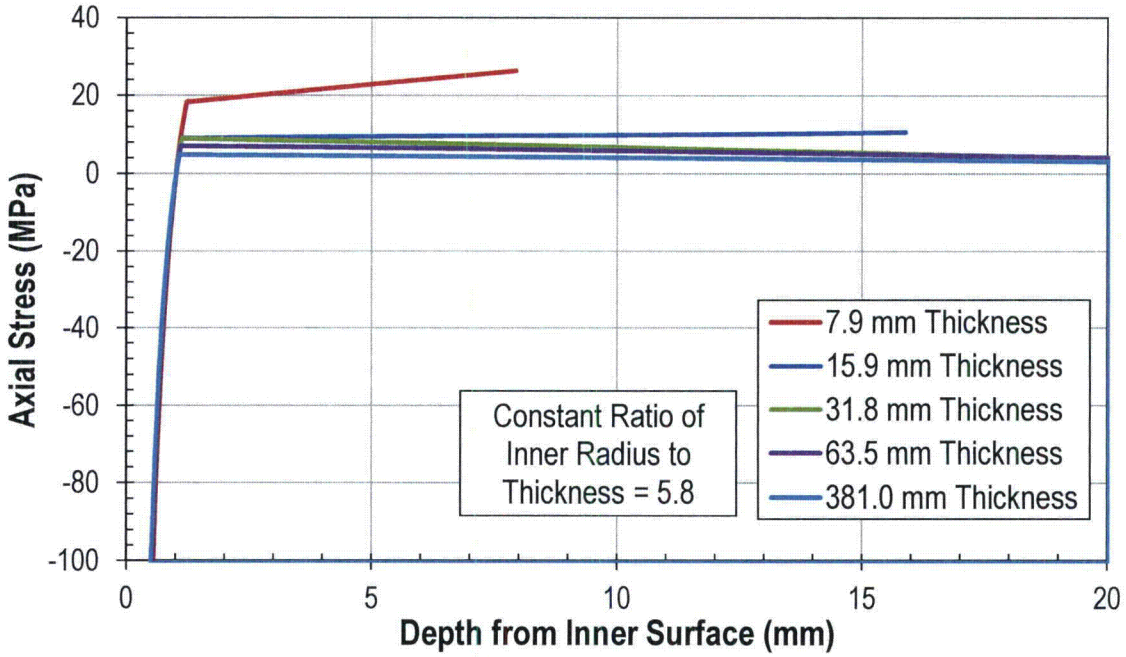

Figure C-8
Effect of Wall Thickness on Through-Wall Axial Stress Profile for Constant R_i / t Pipe Geometry for Same Equilibrium Surface Compressive Stress and Compressive Depth

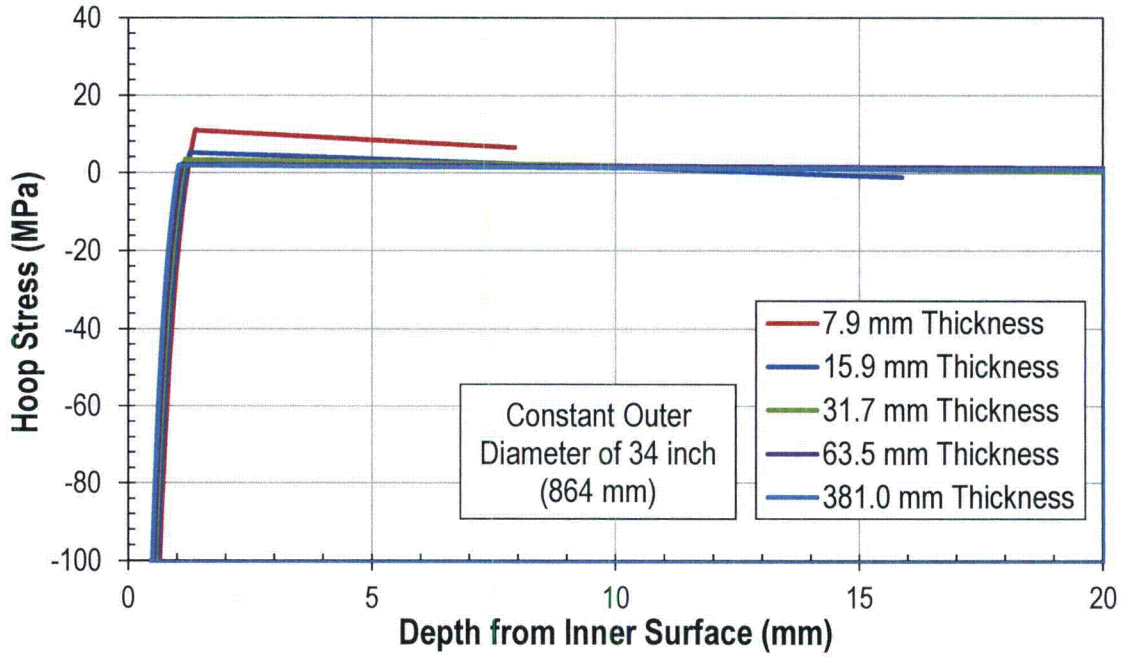

Figure C-9
Effect of Wall Thickness on Through-Wall Hoop Stress Profile for Constant Outer Diameter Pipe Geometry for Same Equilibrium Surface Compressive Stress and Compressive Depth

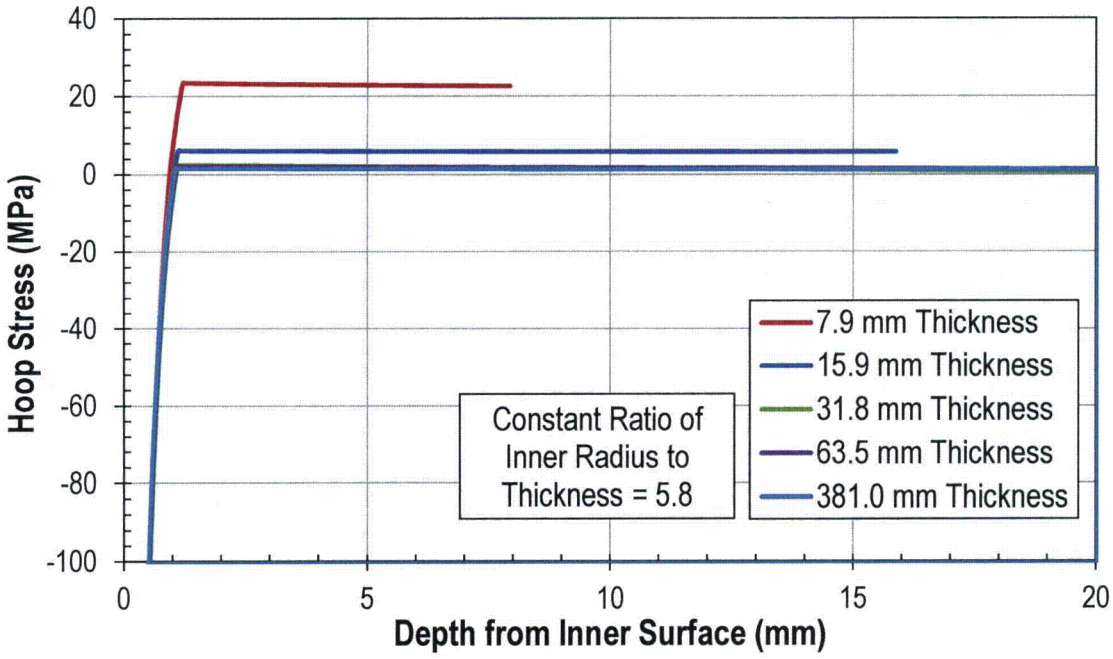

Figure C-10
Effect of Wall Thickness on Through-Wall Hoop Stress Profile for Constant R_i / t Pipe Geometry for Same Equilibrium Surface Compressive Stress and Compressive Depth

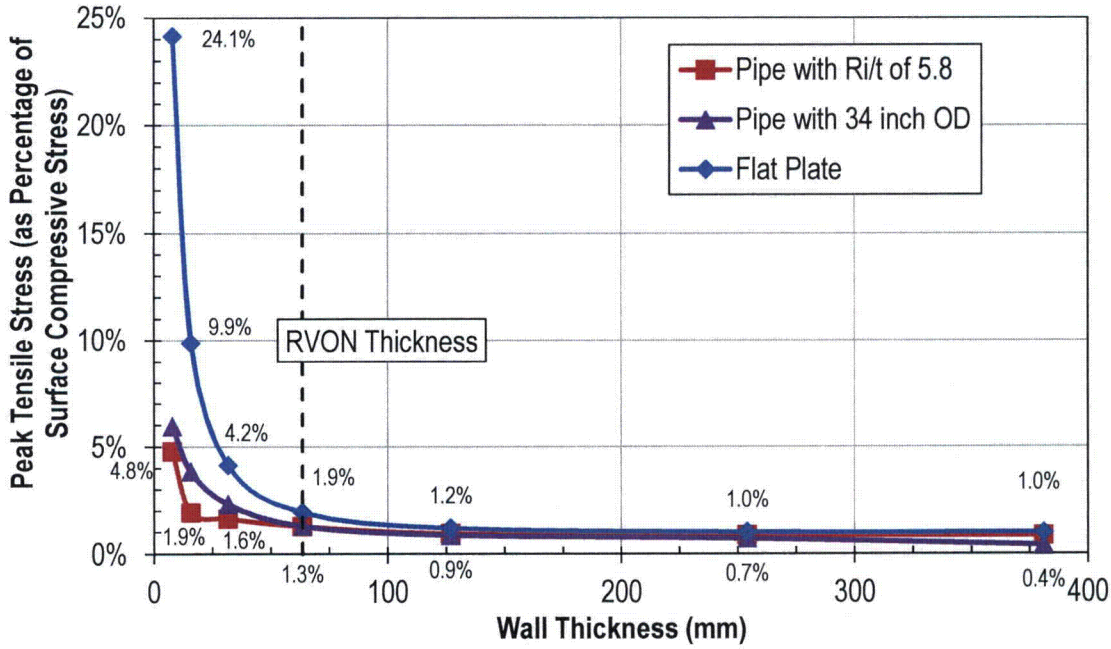

Figure C-11
Effect of Wall Thickness on Peak Tensile Axial Stress for Same Equilibrium Surface Compressive Stress and Compressive Depth

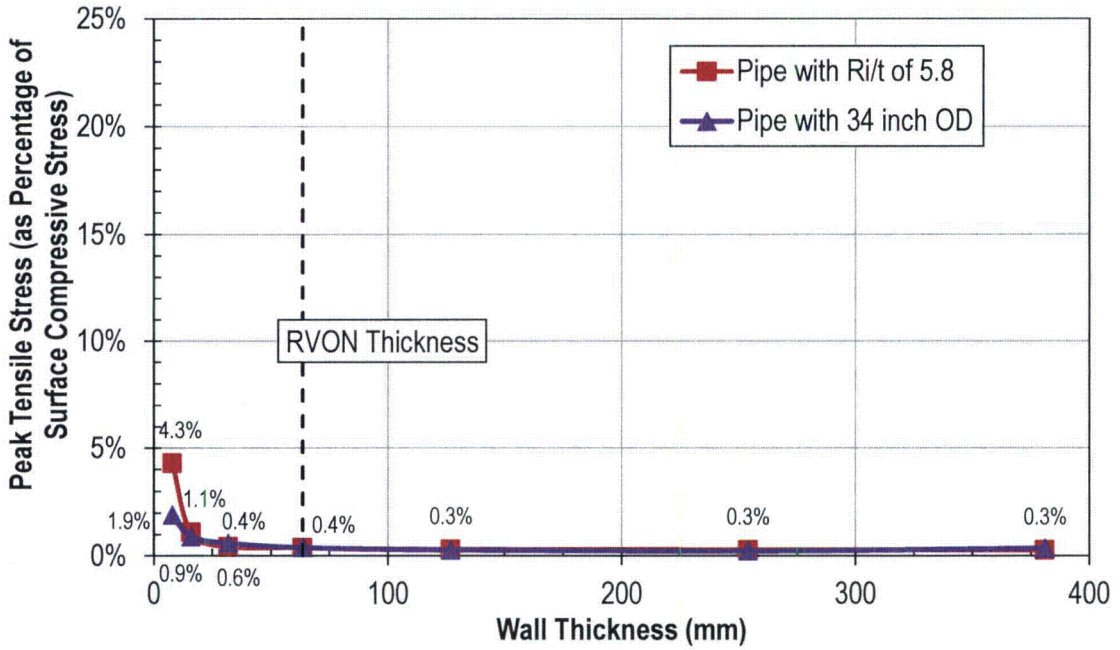

Figure C-12
Effect of Wall Thickness on Peak Tensile Hoop Stress for Same Equilibrium Surface Compressive Stress and Compressive Depth

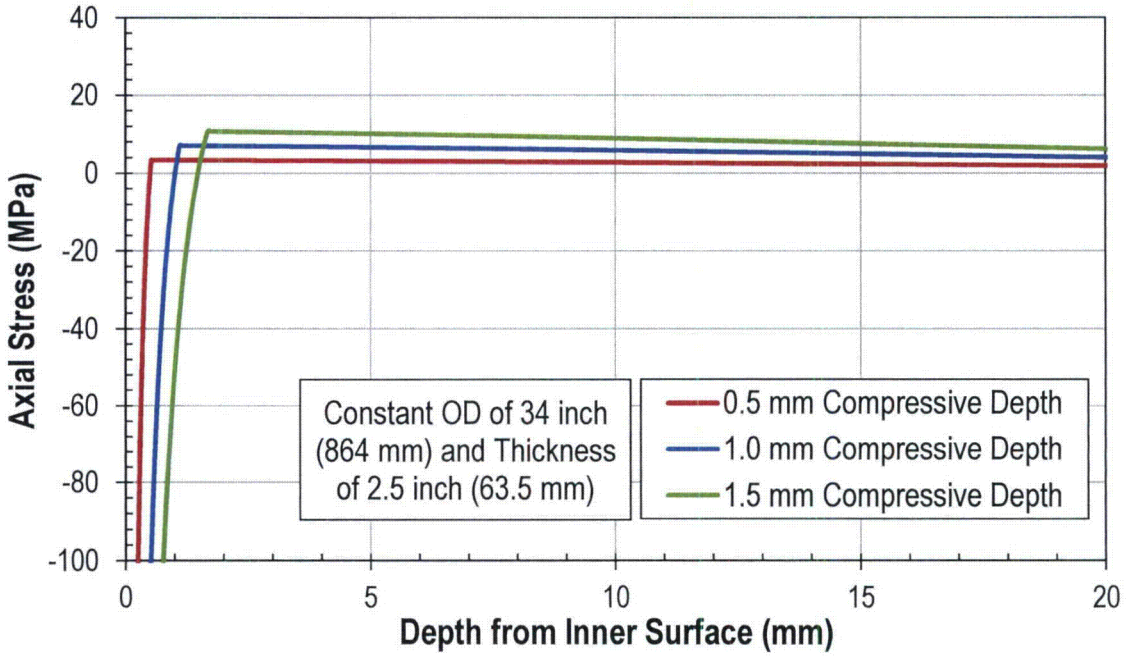

Figure C-13
Effect of Compressive Stress Depth on Through-Wall Axial Stress Profile for RVON Pipe Geometry (Surface Stress Held Constant)

C.5 Model Validation Using Bilinear Stress Profile

The ANSYS model is validated by comparing the resulting stresses to a simple piecewise linear stress profile. The piecewise linear stress profile, which ensures that the applicable force and moment balances are satisfied for the simplest possible profile, is subject to the following assumptions:

1. The profile models the effect of peening only.
2. The compressive surface stress is set to an assumed value, $\sigma(x=0)=\sigma_0$.
3. The stress profile transitions to tensile stresses at a pre-defined point, x_0. This is where $\sigma(x=x_0)=0$.
4. The internal forces must balance to zero through the thickness of the peened component assuming that the profile is uniform over the cross section of an unrestrained flat plate:

$$F_{net}=\int_0^t \sigma(x)dx=0 \qquad \text{[C-3]}$$

5. The internal moments must balance to zero though the thickness of the peened component assuming that the profile is uniform over the cross section of an unrestrained flat plate:

$$M_{net}=\int_0^t x\sigma(x)dx=0 \qquad \text{[C-4]}$$

The piecewise linear stress profile is defined by two line segments; the first is defined by assumptions (2) and (3), whereas the second is defined by assumptions (4) and (5). For the case of the axial stress profile of a thick-wall pipe, Equations [C-3] and [C-4] are assumed to hold except that the force and moment integration are each weighted by the radial coordinate to account for the increase in cross sectional area toward the OD. In each validation case, the values of σ_0 and x_0 were selected to match the FEA profile.

Figure C-14 and Figure C-15 compare the bilinear profile with the FEA results for two cases.

- Figure C-14 shows reasonable agreement versus the FEA solution and measured stress profile for the flat plate case investigated by Hill et al. [5], including similar peak tensile stress values.
- Figure C-15 shows a similar peak tensile stress for the FEA case investigated for a thick-wall pipe with dimensions applicable to reactor vessel outlet and inlet nozzles. The somewhat smaller peak stress for the FEA case is the result of the curvature in the FEA stress profile close to the peened surface. This curvature results in a reduced force and a reduced moment to be balanced by the remainder of the stress profile. This particular FEA stress profile is from a region with a rather uniform curvature that is close to a through-wall moment balance without considering the effect of shear stress on the moment balance.

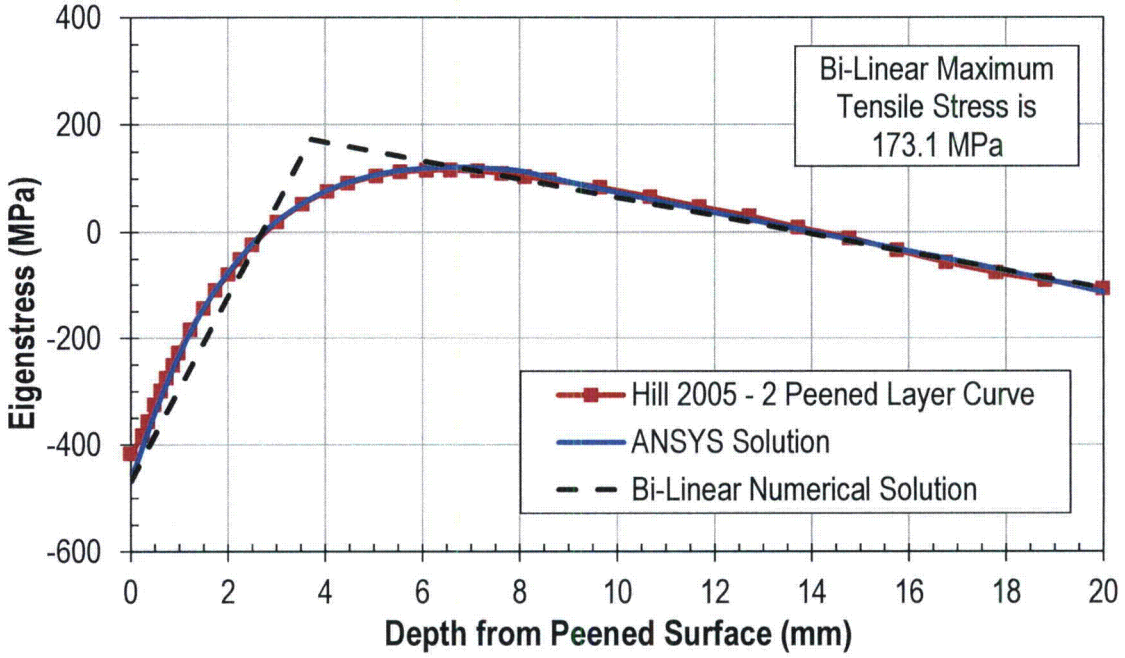

Figure C-14
ANSYS Model Validation for Profile Measured by Hill et al. [5] Using Bilinear Stress Profile

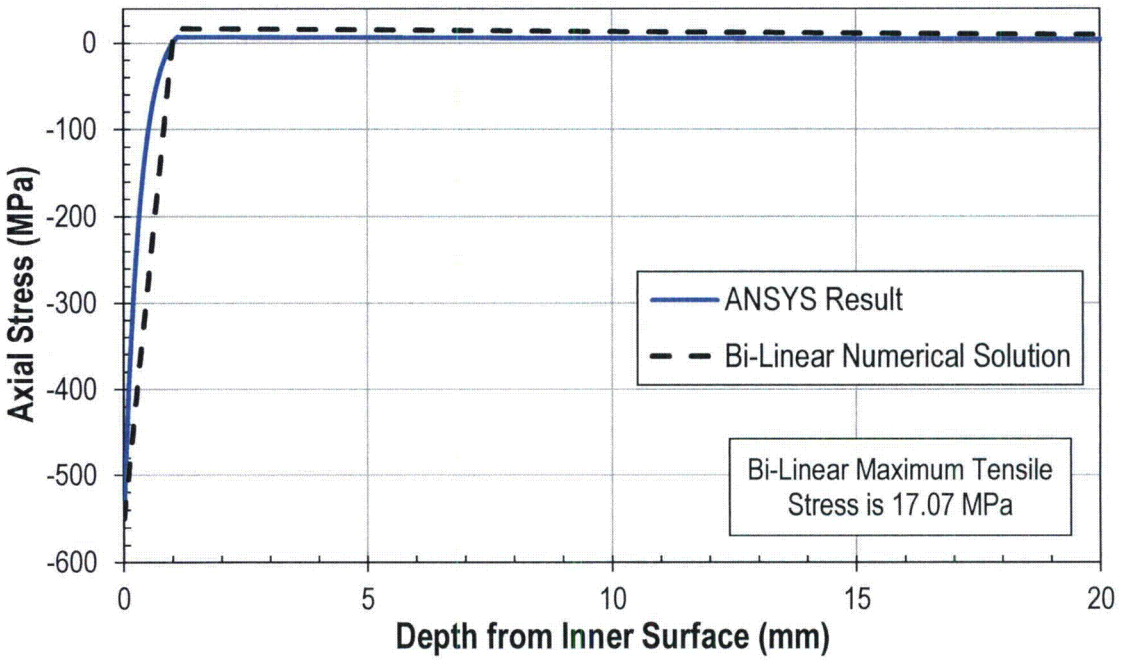

Figure C-15
ANSYS Model Validation for Reactor Vessel Outlet Nozzle (RVON) Case Using Bilinear Stress Profile

C.6 Conclusions

The literature review and analyses presented in this attachment demonstrate the following:

- A balancing stress profile develops beyond the compressive residual stress induced by peening at the treated surface. This balancing stress consists of a through-wall bending component and an axial membrane stress. These residual stress components act to balance the force and change in curvature associated with the peening compressive residual stress developed in the region of the treated surface. The peak tensile stress generally forms in the region just beyond the peening compressive stress layer. The peak tensile stress location represents the location beyond the compressive stress zone where the through-wall bending stress is maximum.
- For a given compressive residual stress effect (surface magnitude and depth of compression) retained upon peening, the peak tensile balancing stress decreases as the component thickness increases. As the component thickness increases, the balancing force and moment are each spread over a greater distance. The difference in balancing stress required to develop the balancing through-wall moment is decreased. The increase in moment arm distance means that a smaller stress difference will create the same moment. Similar trends are produced for thick-wall pipes peened on the inside diameter as for flat plates.
- The peak balancing tensile stress for the case of a peened thick-wall pipe is reduced compared to an unrestrained flat plate of equivalent wall thickness. This is because the more constrained pipe geometry does not deflect as much as the plate case for equivalent peening compressive stress effect and equivalent wall thickness, corresponding to a reduced through-wall drop in the balancing stress profile. The pipe geometry does not satisfy the moment balance in the same manner as for the unrestrained flat plate as shear stresses contribute to the balance for the pipe. The result is that the balancing stress profile for a thick-wall pipe is more nearly uniform than for the case of an unrestrained flat plate of equivalent wall thickness.
- For the reactor vessel outlet nozzle (RVON) geometry evaluated with the FEA model, the peak tensile balancing stresses are less than about 2% of the magnitude of the compressive surface stress for the case of a compressive stress layer at the pipe ID that is 1 millimeter deep. This relatively small magnitude for the peak tensile balancing stress is the result of the balancing force and moment being spread over the large wall thickness of this component, plus the fact that the pipe geometry is more constrained than a flat plate and does not deflect as much as the plate case for equivalent peening compressive stress effect and equivalent wall thickness.

In summary, because of the thick-wall for reactor vessel outlet and inlet nozzles, peening of these components has a small effect on the peak tensile stress below the surface compressive stress zone. With regard to reactor pressure vessel head penetration nozzles (RPVHPNs), the effective thickness of the nozzle at the weld elevation is increased by the presence of the J-groove weld and head. This effect tends to limit the peak tensile balancing stress near the peened ID at the weld elevation. Below the J-groove weld, both the OD and ID surfaces are peened, tending to make the balancing stress uniform over the wall thickness.

C.7 References

1. J. Bernasconi and M. Roth, "The Niku-Lari Method and the Stress Source Method: Application to Residual Stress Distribution of Shot Peened Plates," *Advances in Surface Treatments, Residual Stresses*, Vol. 4, pp. 221-250, Pergamon Press, 1987.
2. S. T. S. Al-Hassani, "Mechanical Aspects of Residual Stress Development in Shot Peening," *Proceedings of ICSP-1*, edited by A. Niku-Lari, pp. 583-602, Pergamon Press, 1981.
3. A. Niku-Lari, "Methode De La Fleche Methode De La Source Des Contraintes Residuelles," *Proceedings of ICSP-1*, edited by A. Niku-Lari, pp. 237-247, Pergamon Press, 1981.
4. D. J. Buchanan and R. John, "Residual Stress Redistribution in Shot Peened Samples Subject to Mechanical Loading," *Materials Science & Engineering A*, Vol. 615, pp. 70-78, 2014.
5. M. R. Hill, et al., "Measurement of Laser Peening Residual Stresses," *Journal of Materials Science & Technology*, Vol. 21, No. 1, pp. 3-9, 2005.
6. R. Menig, et al., "Depth Profiles of Macro Residual Stresses in Thin Shot Peened Steel Plates Determined by X-Ray and Neutron Diffraction," *Scripta Materialia*, Vol. 45, No. 8, pp. 977-983, 2001.
7. A. T. DeWald and M. R. Hill, "Eigenstrain-Based Model for Prediction of Laser Peening Residual Stresses in Arbitrary Three-Dimensional Bodies. Part 2: Model Verification," *Journal of Strain Analysis for Engineering Design*, Vol. 44, No. 1, pp. 13-27, 2009.
8. ANSYS Version 15.0, Mallett Technology, Inc., Canonsbug, PA: 2015.
9. ASME Boiler and Pressure Vessel Code, Section II, Materials, Part D, Properties (Customary), ASME, 2013 Edition, July 1, 2013.
10. *Materials Reliability Program: Alloy 82/182 Pipe Butt Weld Safety Assessment for the US PWR Plant Designs: Westinghouse and CE Design Plants (MRP-109NP)*, EPRI, Palo Alto, CA: 2004. 1009804. [NRC ADAMS Accession No. ML042430093]
11. *Materials Reliability Program: Technical Basis for Primary Water Stress Corrosion Cracking Mitigation by Surface Stress Improvement (MRP-267, Revision 1)*, EPRI, Palo Alto, CA: 2012. 1025839. [Freely Available at www.epri.com]